In-plane bending behaviour of S690 high strength steel welded I-section beams

Yao Sun [a], An He [a], Yating Liang [b], Ou Zhao [*a]

[a] School of Civil and Environmental Engineering, Nanyang Technological University, Singapore

[b] School of Engineering, University of Glasgow, Glasgow, UK

[*] Corresponding author, Phone: +65 6790 6934

Email: ou.zhao@ntu.edu.sg

Abstract

The present paper describes an in-depth experimental and numerical investigation into the in-plane flexural behaviour and bending moment resistances of S690 high strength steel welded I-section beams. The experimental investigation was conducted on six different welded I-sections fabricated from the same batch of 5 mm thick S700MC high strength steel hot-rolled plated by means of gas metal arc welding, and involved initial local geometric imperfection measurements and twelve in-plane four-point bending tests, with six performed about the cross-section major principal axes and another six conducted about the cross-section minor principal axes. Following the experimental study, a numerical investigation was performed, where the developed finite element models were firstly validated against the test results and then used to perform parametric studies to generate further structural performance data over a broader range of cross-section sizes. The obtained experimental and numerical results were carefully analysed and then adopted to evaluate the accuracy of the existing slenderness limits (for classifications of plate elements and cross-sections) and local buckling design rules for S690 high strength steel welded I-sections in bending, as set out in the European, Australian and American standards. The results of the evaluation revealed that the codified slenderness limits are generally safe when used for the classification of the constituent plate elements of the examined S690 high strength steel welded I-section beams, except for that given in the American specification for slender/non-slender outstand elements in compression. All of the three considered design standards were shown to yield accurate cross-section bending moment capacity predictions for compact (Class 1 and 2) S690 high strength steel welded I-section beams bent about both the principal axes and non-compact (Class 3) S690 high strength steel welded I-section beams bent about the major principal axes, but resulted in a rather high level of conservatism in predicting the cross-section bending moment capacities for non-compact (Class 3) S690 high strength steel welded I-sections in bending about the minor principal axes and slender (Class 4) S690 high strength steel welded I-sections subjected to both major-axis bending and minor-axis bending.

Keywords: Cross-section bending moment resistances; Cross-section classification; Finite element modelling; Four-point bending tests; High strength steel grade S690; In-plane bending behaviour, International design standards; Welded I-sections

1. Introduction

High strength construction materials have been increasingly used in bridge and structural engineering. Compared with normal strength mild steels (e.g., grades S235, S275 and S355), high strength steels (with the nominal yield strengths greater than 460 MPa) possess superior mechanical strengths, and enable the achievement of structural components designed with smaller cross-section sizes and lighter self-weights, which lead to structures with (i) more usable interior space between vertical and horizontal components and (ii) lighter overall weight, resulting in great savings in the costs of foundations and reduction in seismic loads. However, high material strength is accompanied by low material ductility, and thus high strength steels are not desirable for fabricating beam-to-columns joints, where the rotation capacity (largely dependent on the material ductility) is a major design concern. The lack of experimental verification of high strength steel structural members and joints at present limits the actual application of high strength steel in construction engineering. Experimental investigations have therefore been prompted to verify the structural behaviour of various types of high strength steel components (e.g., stub columns [1–4], long columns [5–9] and beam-columns [10]) of I-shaped sections, quantify their cross-section (or member) capacities, and develop precise design approaches. However, it is worth noting that research into S690 high strength steel welded I-section beams remains relatively scarce, despite three previous studies carried out by McDermott [11], Beg and Hladnik [12] and Wang [13].

To expand the experimental and numerical data pool on S690 high strength steel welded I-section beams and further examine their flexural behaviour and strengths, a thorough testing and finite element simulation study was conducted and presented in this paper. An experimental study was firstly conducted on six S690 high strength steel welded I-sections, and involved initial local geometric imperfection measurements and twelve in-plane four-point bending tests, with six bent about the major principal axes and another six bent about the minor principal axes. This was followed by a numerical modelling investigation, where finite element models were firstly developed and validated against the test results and afterwards used to conduct parametric studies, aiming at generating additional numerical data over a broader range of section sizes. Finally, the experimentally and numerically obtained results were used to assess the accuracy of the local buckling design rules for S690 high strength steel welded I-section beams, specified in the European code EN 1993-1-12 [14], Australian standard AS 4100 [15] and American specification ANSI/AISC 360-16 [16].

2. Experimental study

2.1. General

A structural testing programme was performed to examine the in-plane bending behaviour and capacities of S690 high strength steel welded I-section beams. Six different I-section sizes were adopted in the present testing programme: I-50×50×5, I-70×70×5, I-80×60×5, I-90×70×5, I-100×100×5 and I-140×70×5, and all the I-sections were fabricated from the same batch of 5 mm thick S700MC high strength steel hot-rolled plates by gas metal arc welding. Overall, the testing programme involved twelve in-plane four-point bending tests, with six performed about the major principal axes and another six conducted about the minor principal axes, together with the initial local geometric imperfection measurements of the beam specimens.

2.2. Measurements on material properties and membrane residual stresses

Prior to in-plane four-point bending tests, material testing was carried out to derive the material stress–strain responses of the examined S690 high strength steel and measurements on membrane residual stresses were conducted to determine their distributions and amplitudes in S690 high strength steel welded I-sections. The test rigs and procedures were fully reported in Sun et al. [3], with only a brief summary provided herein. Two longitudinal coupons and two transverse coupons were extracted from the same batch of S700MC plates as that used for fabricating the beam specimens, and tested utilising a Schenck 250 kN hydraulic testing machine under displacement control, with the resulting strain rates being in conformity with the specific requirements given in EN ISO 6892-1 [17]. Fig. 1 [3] shows the stress–strain curves measured from both the longitudinal and transverse coupons, while the key average measured material properties, including the Young's modulus E, the yield stress f_y, the ultimate stress f_u, the ultimate-to-yield stress ratio f_u/f_y, the strain at the ultimate stress ε_u and the fracture strain ε_f, are reported in Table 1. The membrane residual stress magnitudes and distributions in the examined S690 high strength steel welded I-sections were measured by means of the sectioning method, with the rig and procedures being in compliance with those recommended in Ziemian [18]. On the basis of the experimental results, a new predictive model [3] was proposed specifically for predicting the membrane residual stresses in S690 high strength steel welded I-sections, with the distribution pattern shown in Fig. 2 and the amplitudes of the peak membrane residual stresses presented in Table 2.

2.3. Measurements on initial local geometric imperfections

Initial geometric imperfections are primarily introduced into steel components during the manufacturing process, and may result in premature failure of the steel components with low load-carrying capacities and steep post-ultimate load–deformation responses. The focus of the present study is on the in-plane flexural (local buckling) behaviour of S690 high strength steel welded I-section beams, and thus the initial local geometric imperfection of each specimen was measured, based on the test rig shown in Fig. 3, where the specimen is clamped on the base table of a milling machine, whilst an LVDT is attached to the head of the milling machine and moved along the centreline of each of the three constituent plates (i.e. one web and two flanges) of the specimen to measure the local deviations [19]. It is worth noting that imperfection measurements were all carried out over the central 75% of the specimen lengths, in order to eliminate the effect of flaring of specimen ends upon cutting. For each constituent plate element of the S690 high strength steel welded I-section beam specimen, the maximum initial local geometric imperfection amplitude was taken as the largest deviation from a linear regression surface fitted to the corresponding measured data set [20–23], and presented in Table 3, where ω_w, ω_{f1}, ω_{f2} are the measured maximum local imperfection amplitudes of the web and two flanges, respectively, while the initial local geometric imperfection amplitude of the S690 high strength steel welded I-section beam specimen ω_0 was taken as the maximum of ω_w, ω_{f1} and ω_{f2}.

2.4. Four-point bending tests

For each S690 high strength steel welded I-section, two four-point bending tests were conducted about both the major and minor principal axes, to study the in-plane flexural behaviour and bending moment resistances. The member lengths and cross-section geometric sizes of the beam specimens were carefully measured, and presented in Table 3, where L is the specimen length, h is the outer section depth, b_f is the flange width and t is the wall thickness. The four-point bending test procedures and setup conformed to those recommended in Ziemian [18]. Displacement-controlled loading scheme was adopted to drive the actuator of an INSTRON 2000 kN hydraulic testing frame, with a constant speed of 2 mm/min. Fig. 4 shows the setup for the four-point bending tests about the minor principal axes, where two pairs of steel rollers are employed to provide the four-point bending configuration, with one pair located at a distance of 50 mm from the end sections of the beam specimen and the other pair placed at third-points of the flexural span (i.e. the span between the two end rollers) of the beam specimen, solid wooden blocks are inserted into the beam specimen at the two loading points as well as the two supports, in order to avoid the occurrence of crippling failure of flanges, and three string potentiometers are placed at the two loading points and mid-span to record the respective vertical deflections. The four-point bending tests about the major principal axes were performed using a similar test rig, as shown in Fig. 5, but with G-clamps vertically mounted onto the spreader beam to act as lateral restraints for preventing any lateral or torsional deformation of the beam specimens and eliminating the possibility of member lateral-torsional buckling.

All the tested S690 high strength steel welded I-section beam specimens exhibited visible in-plane deformation and failed by local buckling; Fig. 6 and Fig. 7 depict the failure modes of typical beam specimens I-100×100×5-MA (in major-axis bending) and I-100×100×5-MI (in minor-axis bending), respectively. The key test results, obtained from the four-point bending tests, are presented in Table 4, including the failure moment M_u, the ratios of M_u/M_{pl} and M_u/M_{el}, in which M_{pl} and M_{el} are the cross-section plastic and elastic moment resistances with respect to the considered bending axis, and respectively calculated as the plastic (W_{pl}) and elastic (W_{el}) section moduli multiplied by the material yield stress f_y, and the beam rotation capacity R [24–26]. Figs 8 and 9 depict the normalised moment–curvature curves for the examined S690 high strength steel welded I-section beam specimens in major-axis bending and in minor-axis bending, respectively, where the curvature κ is calculated from Eq. (1), in which D_L and D_M are the corresponding vertical deflections at the loading points and at the mid-span, as measured from the string potentiometers, and L_m is the distance between the two loading points.

$$\kappa = \frac{8\left(D_M - D_L\right)}{4\left(D_M - D_L\right)^2 + L_m^2} \qquad (1)$$

3. Numerical investigation

3.1. General

In conjunction with the structural testing performed in Section 2, a numerical modelling study was performed, utilising the nonlinear finite element (FE) software ABAQUS [27], and reported in the present section. A numerical validation study was initially conducted to validate the developed FE models against the obtained experimental results, followed by a parametric study to derive additional numerical results on S690 high strength steel welded-I-section beams over a wider spectrum of cross-section sizes.

3.2. Development of finite element (FE) models

Having been successfully and widely utilised in previous numerical modelling of high strength steel welded I-section members [3,28,29], the four-node shell element S4R [27] was also employed herein for simulating S690 high strength steel welded I-section beams. The element size was selected upon a mesh sensitivity study examining a range of element sizes from $0.5t$ to $3t$; it was generally found that an element size equal to the material thickness t led to accurate incorporation of the membrane residual stresses into the FE models and also resulted in both precise numerical results and adequate computational efficiency, and was thus assigned to each beam FE model. The stress–strain curves, measured from the longitudinal coupons, were firstly converted into the true stress–true plastic strain curves and then inputted into ABAQUS [27].

The membrane residual stress distributions and amplitudes, as derived from the proposed predictive model [3] (see Section 2.2), were incorporated into the beam FE models through the '*INITIAL CONDITIONS' command [27]; Fig. 10 displays a typical membrane residual stress pattern incorporated into the FE models for the beam specimens I-100×100×5-MA and I-100×100×5-MI.

For the ease of setting boundary conditions, each of the two sections of the beam FE models at the end supports was coupled to a reference point, positioned at the bottom web-to-flange junction for major-axis bending or at the mid-point between the two bottom flange tips for minor-axis bending. In order to replicate the simply-supported boundary condition used in the testing, one reference point was allowed to translate longitudinally and rotate about the axis of bending while the other one was only allowed for rotation about the same bending axis. Besides, the cross-section at each loading point was also coupled to a reference point, which was located at the top web-to-flange junction for major-axis bending or at the mid-point between the two top flange tips for minor-axis bending, and allowed to have translations along both the longitudinal and vertical directions and rotation about the axis of bending, to mimic the four-point bending configuration. With regards to the modelling of beams bent about the major principal axes, additional lateral and torsional restraints were applied to those cross-sections that were restrained by G-clamps in the testing, to eliminate the possibility of lateral-torsional buckling.

Initial local geometric imperfections were incorporated into the S690 high strength steel welded I-section beam FE models, with the distribution patterns taken as the lowest elastic buckling mode shapes in four-point bending and derived from a prior elastic eigenvalue buckling analysis [30–35]. Four initial local imperfection amplitudes, including the measured imperfection value ω_0 and 1/10, 1/30 and 1/100 of material thickness t, were then used to factor the derived imperfection patterns, enabling the sensitivity of the established S690 high strength steel weld I-section beam FE models to imperfection amplitudes to be evaluated.

3.3. Validation of finite element models

Upon establishment of the S690 high strength steel welded I-section beam FE models, nonlinear static Riks analysis [27] was conducted to determine the numerical ultimate bending moments, moment–curvature responses and failure modes. Based on the comparisons of the numerical results against their experimental counterparts, the accuracy of the established beam FE models was evaluated. The FE to experimental ultimate moment ratios for the tested S690 high strength steel welded I-section beam specimens are reported in Table 5, in which the results generally indicate that all the four adopted initial local geometric imperfection amplitudes yield precise and consistent predictions of the experimental failure moments, with the best agreement obtained when the local imperfection amplitude equal to 1/100 of the material thickness was used in the numerical simulation. Figs 6 and 7 depict the comparisons between the experimental and numerical local buckling failure modes for typical beam specimens I-100×100×5-MA and I-100×100×5-MI subjected to major-axis bending and minor-axis bending, respectively, indicating excellent agreement. The experimentally and numerically derived normalised moment–curvature responses for a typical beam specimen I-140×70×5-MA in major-axis bending are compared in Fig. 11, while a similar graphic comparison is shown in Fig. 12 for a typical beam specimen I-100×100×5-MI in minor-axis bending, both revealing that the established beam FE models are capable of replicating the full experimental normalised moment–curvature histories. Moreover, the normalised numerical moment–curvature curves were also derived from the beam FE models without inclusion of membrane residual stresses and shown in Figs 11 and 12; the normalised numerical moment–curvature responses with and without membrane residual stresses were observed to almost coincide, revealing that the effect of membrane residual stresses on the in-plane bending behaviour of S690 high strength steel welded I-section beams is negligible, as also highlighted in previous similar numerical studies [33,35]. In sum, the developed beam finite element models have been proven to be capable of precisely simulating the four-point bending tests on S690 high strength steel welded I-section beams.

3.4. Parametric studies

On the basis of the beam FE models established and validated in Section 3.3, parametric studies were performed to derive additional numerical data beyond those derived from the experiments. In the present parametric studies, the material stress–strain responses measured from the longitudinal coupons were employed, while the incorporated initial local imperfection amplitudes were selected as $t/100$. The flexural spans of all the numerically modelled I-section beams were equal to 1500 mm, whilst the two loading points were positioned at third-points of the flexural spans. Regarding the cross-section sizes of the modelled I-section beams, the outer depths were fixed at 150 mm, with the flange widths taken as 75 mm, 100 mm and 150 mm, respectively, resulting in a range of cross-section aspect ratios being considered; the thicknesses of the web and flanges of each modelled I-section were set to be equal and varied between 2 mm and 15 mm, which led to a broad spectrum of cross-section geometric sizes being examined. In total, 185 and 101 numerical data on S690 high strength steel welded I-section beams under major-axis and minor-axis bending were respectively generated through parametric studies.

4. Assessment of existing international design codes

4.1. General

In the present section, the beam test results, obtained in Section 2, together with the numerical data, acquired in Section 3, were used to evaluate the accuracy of the slenderness limits and design rules for S690 high strength steel welded I-section beams susceptible to in-plane bending failure, as specified in the existing European code EN 1993-1-12 [14], Australian standard AS 4100 [15] and American Specification ANSI/AISC 360-16 [16]. The unfactored design cross-section bending moment resistances ($M_{u,EC3}$, $M_{u,AS}$ and $M_{u,AISC}$) were firstly calculated in accordance with the three considered design codes and afterwards compared against the test (and numerical) ultimate bending moments, with the mean test (or numerical) to predicted ultimate bending moment ratio ($M_u/M_{u,EC3}$, $M_u/M_{u,AS}$ or $M_u/M_{u,AISC}$) for each design code given in Table 6.

4.2. European code EN 1993-1-12 (EC3)

4.2.1. General

The current Eurocode EN 1993-1-12 [14] was developed specifically for high strength steels with grades greater than S460 up to S700, though mirroring most of the design provisions given in EN 1993-1-1 [36] for normal strength mild steels. Regarding the design of S690 high strength steel welded I-sections subjected to bending, EN 1993-1-12 [14] adopts the same concept of cross-section classification (i.e. the strength of the cross-section is dependent on the class of the cross-section) as that utilised in EN 1993-1-1 [36]. Four cross-section classes were specified in the Eurocodes [14,36]: Class 1 and 2 (plastic) sections in bending can achieve the plastic moment capacities (M_{pl}), Class 3 (elastic) sections subject to bending are capable of attaining the elastic moment capacities (M_{el}), and Class 4 (slender) sections fail before the material yield stresses f_y are attained, with the design bending moment resistances limited to the effective moment capacities (M_{eff}). To determine the class of a welded I-section in bending, all of its constituent plate elements (i.e. outstand flanges and internal web) are firstly classified through comparisons of the respective flat width-to-thickness ratios (c_w/t and c_f/t, in which c_w and c_f are respectively the flat widths of the web and flange) against the slenderness limits specified in the Eurocodes [14,36], and the class of the most slender plate element is then defined as the overall class of the examined I-section. The EC3 Class 3 and Class 2 slenderness limits for classifying internal and outstand plate elements under various loading conditions (i.e.

compression, bending and compressive stress gradients) are listed in Table 7(a), where ε_{EC3}= $\sqrt{235/f_y}$ is the EC3 material parameter to consider the effect of material strength on the plate element slenderness limits, and k_σ is the buckling factor and dependent on the stress distribution and boundary condition of the plate element. In the following sub-section 4.2.2 and sub-section 4.2.3, the accuracy of the EN 1993-1-12 slenderness limits and design bending moment capacities were respectively evaluated.

4.2.2. Cross-section classification limits

The Class 3 slenderness limits for outstand plate elements in compression and internal plate elements in bending were assessed based on the experimental and FE data on S690 high strength steel welded I-section beams bent about the major principal axes, with the results of the graphic assessments respectively depicted in Fig. 13 and Fig. 14, where the test and numerical ultimate bending moments, normalised by the cross-section elastic moment resistances, are plotted against the $c_f/(t\varepsilon_{EC3})$ and $c_w/(t\varepsilon_{EC3})$ ratios of the examined S690 high strength steel welded I-sections, together with the EC3 Class 3 slenderness limits (normalised by ε_{EC3}) for outstand plate elements in compression $c_f/(t\varepsilon_{EC3})$=14 and internal plate elements in bending $c_w/(t\varepsilon_{EC3})$=124. It was generally found that the established Class 3 slenderness limits in EN 1993-1-12 [14] are safe but conservative when used for the classification of internal webs (in bending) and outstand flanges (in compression) of S690 high strength steel welded I-sections subjected to major-axis bending. The ultimate bending moment resistances, derived from the structural testing and finite element modelling on S690 high strength steel welded I-section beams in minor-axis bending, were then utilised to assess the accuracy of the current EC3 Class 3 slenderness limit for outstand plate elements under triangular compressive stress gradients ($c_f/(t\varepsilon_{EC3})=21k_\sigma^{0.5}$, in which $k_\sigma=0.57$) in Fig. 15. The results of the assessments generally revealed that the EC3 Class 3 slenderness limit for outstand plate elements under triangular compressive stress gradients is rather conservative though safe when used for the classification of outstand flanges of S690 high strength steel welded I-section beams in minor-axis bending.

A similar graphic evaluation was also performed on the established EC3 Class 2 slenderness limit for internal plate elements in bending ($c_w/(t\varepsilon_{EC3})=83$), based on the test and numerical data on S690 high strength steel welded I-section beams under major-axis bending, as given in Fig. 16. The EC3 Class 2 slenderness limits for outstand plate elements in compression ($c_f/(t\varepsilon_{EC3})=10$) was evaluated, based on the derived experimental and FE data on S690 high strength steel welded I-section beams bent about both the major and minor principal axes, as depicted in Fig. 17. The results of the graphic evaluations in Figs 16 and 17 generally revealed that the Class 2 slenderness limits established in EN 1993-1-12 [14] are safe and accurate when used for the classifications of internal webs (in bending) and outstand flanges (in compression) of S690 welded I-section beams.

4.2.3. EC3 Cross-section bending moment resistance predictions

The EC3 predictions of cross-section bending moment capacities for S690 high strength steel welded I-section beams were assessed through comparisons against the obtained test and FE ultimate bending moments. The current EN 1993-1-12 [14] prescribes the use of cross-section plastic (M_{pl}) and elastic (M_{el}) moment capacities as the design bending moment capacities for Class 1 (and 2) and Class 3 sections, respectively, and adopts the effective width method to predict the cross-section bending moment resistances for those slender Class 4 sections. The effective width method makes due allowance for loss of effectiveness owing to local buckling by reducing the flat widths of the slender constituent outstand and internal plate elements. The effective (reduced) widths c_{eff} of slender flanges (outstand elements) and webs (internal elements) of I-sections can be respectively calculated from Eq. (2) and Eq. (3) [37], in which $\bar{\lambda}_p$ is the slenderness of the plate element, as defined by Eq. (4), where k_σ is the buckling factor, dependent on the type of the plate element and stress distribution throughout plate width, and can be calculated in accordance with Tables 4.1 and 4.2 of EN 1993-1-5 [37]. Upon calculation of the effective widths of all the slender plate elements of the Class 4 welded I-section, the EC3 effective section modulus ($W_{eff,EC3}$) and effective bending moment capacity ($M_{eff,EC3}=W_{eff,EC3}f_y$) can then be derived; it is worth noting that cumbersome iterations may be involved in the calculation of $W_{eff,EC3}$ due to the shift in effective neutral axis along with each round of calculation.

$$c_{eff} = c_f\left(\frac{1}{\bar{\lambda}_p} - \frac{0.188}{\bar{\lambda}_p^2}\right) \le c_f \tag{2}$$

$$c_{eff} = c_w\left(\frac{1}{\bar{\lambda}_p} - \frac{0.22}{\bar{\lambda}_p^2}\right) \le c_w \tag{3}$$

$$\bar{\lambda}_p = \frac{c/t}{28.4\varepsilon_{EC3}\sqrt{k_\sigma}} \tag{4}$$

The ratios of the test and FE ultimate bending moments to the EC3 cross-section bending moment resistance predictions are plotted against the c_f/t ratios of the flanges of the examined I-sections, and depicted in Fig. 18, while Table 6(a) presents the mean experimental (and numerical) to EC3 design cross-section bending capacity ratios $M_u/M_{u,EC3}$, together with the corresponding coefficients of variation (COVs), for different classes of S690 welded I-sections in bending. The results of both the graphic and numerical comparisons revealed that the cross-section bending moment resistances are well predicted by the current EN 1993-1-12 [14] for Class 1 (and Class 2) S690 high strength steel welded I-section beams bent about both the principal axes and Class 3 S690 high strength steel welded I-section beams in major-axis bending, while EN 1993-1-12 [14] yields overly conservative bending moment capacity predications for Class 3 S690 high strength steel welded I-section beams bent about the minor principal axes and Class 4 S690 high strength steel welded I-section beams in both major-axis bending and minor-axis bending.

4.3. Australian Standard AS 4100

The current Australian standard AS 4100 [15], which provides design provisions for both normal strength mild steels and high strength steels with grades up to S690, also employs the cross-section classification framework for the design of welded I-section beams failing by local buckling. Through comparisons of the flat width-to-thickness ratios against the slenderness limits for all the constituent plate elements, cross-sections in bending are classified as compact, non-compact and slender sections in AS 4100 [15], corresponding to Class 1 (and 2), Class 3, and Class 4 sections defined in EN 1993-1-12 [14]. Note that the AS 4100 slenderness limits between non-compact and compact plate elements and between slender and non-compact plate elements are respectively termed as the plasticity and yield slenderness limits (corresponding to the EC3 Class 2 and Class 3 slenderness limits), as presented in Table 7(b), where ε_{AS}= $\sqrt{250/f_y}$ is the AS material parameter. Graphic evaluation of the AS yield slenderness limits for outstand elements in compression ($c_f/(t\varepsilon_{AS})$=14), internal elements in bending ($c_w/(t\varepsilon_{AS})$=115) and outstand elements in triangular compressive stress gradients ($c_f/(t\varepsilon_{AS})$=22) as well as the AS plasticity slenderness limits for internal elements in bending ($c_w/(t\varepsilon_{AS})$=82) and outstand elements in compression ($c_f/(t\varepsilon_{AS})$=8) was carried out based on the relevant test and FE data, and shown in Figs 19–23, respectively. The results of the graphic evaluations generally indicated that the current AS yield limits are safe but considerably conservative when used for the classification of both internal webs and outstand flanges of S690 high strength steel welded I-section beams, while the plasticity slenderness limits yield a good level of accuracy in the plate element classification.

The current AS 4100 [15] adopts M_{pl} as the design bending moment resistances for compact welded I-section beams, but with an upper limit of 1.5M_{el}, as given by Eq. (5), and takes into due account partial plasticity in the predictions of cross-section bending moment resistances for non-compact welded I-section beams, with the design formulation shown by Eq. (6), where M_c is taken as the minimum of M_{pl} and 1.5M_{el} of the examined non-compact I-section, λ_s is equal to the c/t ratio of the most slender constituent plate element of the non-compact I-section in bending; note that the most slender constituent plate element is defined as the element with the greatest plate element c/t to yield slenderness limit (see Table 7(b)) ratio, and λ_{sy} and λ_{sp} are the corresponding yield and plasticity limits for the most slender constituent plate element and presented in Table 7(b). Regarding slender welded I-section beams, the effective bending moment resistances, specified in AS 4100 [15], are determined through multiplying the cross-section elastic moment capacities M_{el} by the reduction factor ρ, as given by Eq. (7); note that the reduction factor ρ is calculated as (λ_{sy}/λ_s) and $(\lambda_{sy}/\lambda_s)^2$ for welded I-sections with the most slender plate element being subjected to uniform compression (i.e. major-axis bending case) and stress gradients (i.e. minor-axis bending case), respectively.

$$M_{u,AS} = M_{pl} \le 1.5M_{el} \tag{5}$$

$$M_{u,AS} = M_{el} + \left(M_c - M_{el}\right)\left(\frac{\lambda_{sy} - \lambda_s}{\lambda_{sy} - \lambda_{sp}}\right) \tag{6}$$

$$M_{u,AS} = \rho M_{el} \tag{7}$$

The accuracy of the current Australian standard AS 4100 [15] for the design of S690 high strength steel welded I-section beams failing by local buckling was assessed by comparing the obtained experimental and FE ultimate bending moments with the AS predicted cross-section bending moment capacities. As evident in Fig. 24 and Table 6(b), the current AS 4100 [15] yields accurate and consistent cross-section bending moment capacity predictions for compact S690 high strength steel welded I-section beams in both major-axis bending and minor-axis bending and non-compact S690 high strength steel welded I-section beams subjected to major-axis bending, but excessively under-estimates the cross-section bending moment resistances for non-compact S690 welded I-section beams bent about the minor principal axes and slender S690 high strength steel welded I-section beams in both major-axis and minor-axis bending.

4.4. American specification ANSI/AISC 360-16

The existing American specification ANSI/AISC 360-16 [16], with the scope of application covering steels with grades up to S690, also adopts the cross-section classification framework for the design of welded I-section beams prone to local instability. Through comparisons of the flat width-to-thickness ratios against the corresponding slenderness limits for all the constituent plate elements, the existing ANSI/AISC 360-16 [16] classifies cross-sections subjected to bending as slender, non-compact and compact sections, similar to the current AS 4100 [15]; note that the flat element widths of flanges of I-shaped sections are given as half of the full flange widths in ANSI/AISC 360-16 [16], while the flat element widths of webs are defined as the clear distances between the flanges. The American specification ANSI/AISC 360-16 [16] terms the slenderness limits for slender/non-compact and non-compact/compact plate elements as non-compact and compact limiting width-to-thickness ratios, as listed in Table 7(c), where $\varepsilon_{AISC}=\sqrt{E/f_y}$ is the AISC material parameter and $k_c=4\sqrt{t/c_w}$ is a geometric parameter to account for the influence of the size of the internal web on the slenderness limit of the outstand flange. The test and FE numerical results on S690 welded I-section beams were adopted to evaluate the accuracy of the AISC non-compact limiting width-to-thickness ratios for outstand elements in compression ($c_f/(t\varepsilon_{AISC}k_c^{0.5})$=1.14), internal elements in bending ($c_w/(t\varepsilon_{AISC})$=5.7) and outstand elements in triangular compressive stress gradients ($c_f/(t\varepsilon_{AISC})$=1.0) as well as the compact limiting width-to-thickness ratios for internal elements in bending ($c_w/(t\varepsilon_{AISC})$=3.76) and outstand elements in compression ($c_f/(t\varepsilon_{AISC})$=0.38), with the results of the respective graphic assessments shown in Figs 25–29. It was found that that all the AISC limiting width-to-thickness ratios are safe and generally accurate when used for the classification of plate elements of S690 high strength steel welded I-section beams except for the non-compact limiting width-to-thickness ratios for outstand elements in compression ($c_f/(t\varepsilon_{AISC}k_c^{0.5})$=1.14), which results in unsafe plate element classification.

With regards to welded I-section beams bent about the cross-section major principal axes, ANSI/AISC 360-16 [16] prescribes the use of plastic moment resistances (M_{pl}) as the design bending moment resistances for both compact I-sections and non-compact I-sections with compact outstand flanges and non-compact internal webs, and takes into account partial plasticity in the predictions of bending moment resistances for non-compact I-sections with non-compact outstand flanges and compact or non-compact internal webs, as given by Eq. (8), where λ_{pf} and λ_{rf} are the compact and non-compact limiting width-to-thickness ratios for outstand flanges under compression, respectively, as listed in Table 7(c). The AISC design cross-section effective (reduced) bending moment capacities for slender I-section beams with (i) slender webs and compact flanges, (ii) slender webs and non-compact flanges and (iii) slender flanges are calculated from Eqs (9)–(11), respectively. Regarding welded I-section beams subjected to minor-axis bending, the current ANSI/AISC 360-16 [16] specifies the design cross-section bending moment resistances as the minimum of M_{pl} and $1.6M_{el}$ for compact I-sections, while the design cross-section bending moment resistances of non-compact and slender I-sections are determined according to Eqs (8) and (12), respectively.

$$M_{u,AISC} = M_{pl} - \left(M_{pl} - 0.7M_{el}\right)\left(\frac{c_f/t - \lambda_{pf}}{\lambda_{rf} - \lambda_{pf}}\right) \tag{8}$$

$$M_{u,AISC} = M_{eff,AISC} = M_{el}\left[1 - \frac{c_w/\left(2c_f\right)}{1200 + 300\left(c_w/\left(2c_f\right)\right)}\left(c_w/t - 5.7\varepsilon_{AISC}\right)\right] \le M_{el} \tag{9}$$

$$M_{u,AISC} = M_{eff,AISC} = M_{el}\left[1 - 0.3\left(\frac{c_f/t - \lambda_{pf}}{\lambda_{rf} - \lambda_{pf}}\right)\right] \le M_{el} \tag{10}$$

$$M_{u,AISC} = M_{eff,AISC} = M_{el}\frac{0.9k_c}{\left(c_f/t\varepsilon_{AISC}\right)^2} \le M_{el} \tag{11}$$

$$M_{u,AISC} = M_{eff,AISC} = M_{el}\frac{0.69}{\left(c_f/t\varepsilon_{AISC}\right)^2} \le M_{el} \tag{12}$$

Graphic and quantitative evaluations of the AISC design cross-section bending moment capacities were carried out based on the experimental (and FE) ultimate bending moments of the examined S690 high strength steel welded I-section beams, with the results shown in Fig. 30 and Table 6(c), respectively. It is evident that the test and FE ultimate bending moments of compact S690 high strength steel welded I-section beams (in bending about both the principal axes) and non-compact S690 high strength steel welded I-section beams bent about the major principal axes are well predicted by the current ANSI/AISC 360-16 [16], while the design cross-section bending moment capacity predictions of non-compact S690 high strength steel welded I-section beams in minor-axis bending and slender S690 high strength steel welded I-section beams in both minor-axis and major-axis bending, determined from ANSI/AISC 360-16 [16], are excessively conservative and scattered.

5. Conclusions

A testing and numerical modelling investigation into the in-plane flexural behaviour and bending moment resistances of welded I-section beams made of grade S690 high strength steel has been conducted and described in this paper. The experimental programme was conducted on six different S690 high strength steel welded I-sections, and involved initial geometric imperfection measurements, six four-point bending tests about the major principal axes and six four-point bending tests about the minor principal axes. In parallel with the structural testing, a finite element simulation study was performed, including a validation study to replicate the four-point bending tests on S690 high strength steel welded I-section beams and a parametric sturdy to derive additional finite element data. The obtained test and finite element results were adopted to assess the accuracy of the slenderness limits for the classifications of internal webs and outstand flanges of S690 high strength steel welded I-sections in bending as well as the local buckling design provisions for S690 high strength steel welded I-section beams, as specified in 1993-1-12 [14], AS 4100 [15] and ANSI/AISC 360-16 [16]. The assessment results generally indicated that (i) all the established codified slenderness limits are safe for the classifications of plate elements and cross-sections of S690 high strength steel welded I-section beams, with an exception being the AISC non-compact limiting width-to-thickness ratio for outstand elements in compression, and (ii) the codified local buckling design rules in all the three design standards [14–16] were shown to yield precise and consistent cross-section bending moment capacity predictions for compact (Class 1 and 2) S690 welded I-section beams in bending about both the principal axes and non-compact (Class 3) S690 welded I-sections bent about the major principal axes, while the predicted cross-section bending resistances, determined from all the three design standards [14–16], were unduly conservative for non-compact (Class 3) S690 welded I-sections in minor-axis bending and slender (Class 4) S690 welded I-section beams in both major-axis and minor-axis bending.

Acknowledgements

The research work presented in this paper is funded by the Regency Steel Asia (RSA) Endowment Fund. The authors would like to thank SSAB Swedish Steel Pte Ltd., Singapore for their help in fabricating S690 high strength steel welded I-sections. The authors are also grateful to the assistance from Mr. Subasanran Chelladurai in the tests and to the financial support from NTU Research Scholarship.

References

[1] K.J.R. Rasmussen, G.J. Hancock, Plate slenderness limits for high strength steel sections, J. Constr. Steel Res. 23 (1–3) (1992) 73–96.

[2] G. Shi, W. Zhou, Y. Bai, C. Lin, Local buckling of 460 MPa high strength steel welded section stub columns under axial compression, J. Constr. Steel Res. 100 (2014) 60–70.

[3] Y. Sun, Y. Liang, O. Zhao, Testing, numerical modelling and design of S690 high strength steel welded I-section stub columns, J. Constr. Steel Res. 159 (2019) 521–533.

[4] G. Shi, W. Zhou, C. Lin, Experimental investigation on the local buckling behavior of

960 MPa high strength steel welded section stub columns, Adv. Struct. Eng. 18 (3) (2015) 423–437.

[5] K.J.R. Rasmussen, G.J. Hancock, Tests of high strength steel columns, J. Constr. Steel Res. 34 (1) (1995) 27–52.

[6] G. Shi, H. Ban, F.S.K. Bijlaard, Tests and numerical study of ultra-high strength steel columns with end restraints, J. Constr. Steel Res. 70 (2012) 236–247.

[7] H. Ban, G. Shi, Y. Shi, Y. Wang, Overall buckling behavior of 460 MPa high strength steel columns: Experimental investigation and design method, J. Constr. Steel Res. 74 (2012) 140–150.

[8] T. Li, G. Li, S. Chan, Y. Wang, Behavior of Q690 high-strength steel columns: part 1: experimental investigation, J. Constr. Steel Res. 123 (2016) 18–30.

[9] T. Ma, X. Liu, Y. Hu, K. Chung, G. Li, Structural behavior of slender columns of high strength S690 steel welded H-sections under compression, Eng. Struct. 157 (2018) 75–85.

[10] T. Ma, Y. Hu, X. Liu, G. Li, K. Chung, Experimental investigation into high strength Q690 steel welded H-sections under combined compression and bending, J. Constr. Steel Res. 138 (2017) 449–462.

[11] J.F. McDermott, Plastic bending of A514 steel beams, J. Struct. Div. 95 (9) (1969) 1851–1871.

[12] D. Beg, L. Hladnik, Slenderness limit of Class 3 I cross-sections made of high strength steel, J. Constr. Steel Res. 38 (3) (1996) 201–217.

[13] K. Wang, Study on structural behaviour of high strength steel S690 welded H- and I-

sections, Ph.D thesis, the Hong Kong Polytechnic University (2018).

[14] EN 1993-1-12:2007, Eurocode 3: design of steel structures – Part 1.12: Additional rules for the extension of EN 1993 up to steel grades S 700, European Committee for Standardization (CEN), Brussels, 2007.

[15] AS 4100-1998: Reconfirmed 2016, Steel structures. Australian standard, Committee BD-001, 2016.

[16] ANSI/AISC 360-16, Specification for the Structural Steel Buildings, American Institute of Steel Construction (AISC); 2016.

[17] EN ISO 6892-1, Metallic Matetials: Tensile Testing – Part 1: Method of Test at Room Temperature, European Committee for Standardization (CEN), Brussels, 2016.

[18] R.D. Ziemian, Guide to Stability Design Criteria for Metal Structures, 6th ed. John Wiley & Sons, 2010.

[19] B.W. Schafer, T. Peköz, Computational modeling of cold-formed steel: characterizing geometric imperfections and residual stresses, J. Constr. Steel Res. 47 (3) (1998) 193–210.

[20] O. Zhao, L. Gardner, B. Young, Experimental study of ferritic stainless steel tubular beam-column members subjected to unequal end moments, J. Struct. Eng. ASCE 142 (11) (2016), 04016091.

[21] M. Chen, B. Young, Material properties and structural behavior of cold-formed steel elliptical hollow section stub columns, Thin-Walled Struct. 134 (2019) 111–126.

[22] O. Zhao, B. Rossi, L. Gardner, B. Young, Behaviour of structural stainless steel cross-sections under combined loading – Part I: experimental study, Eng. Struct. 89 (2015)

236–246.

[23] M. Su, B. Young, L. Gardner, Testing and design of aluminum alloy cross sections in compression, J. Struct. Eng. ASCE 140 (9) (2014) 04014047.

[24] O. Zhao, B. Rossi, L. Gardner, B. Young, Experimental and numerical studies of ferritic stainless steel tubular cross sections under combined compression and bending, J. Struct. Eng. ASCE 142 (2) (2016), 04015110.

[25] T.M. Chan, L. Gardner, Bending strength of hot-rolled elliptical hollow sections, J. Constr. Steel Res. 64 (9) (2008) 971–986.

[26] Y. Sun, O. Zhao, Material response and local stability of high-chromium stainless steel welded I-sections, Eng. Struct. 178 (2019) 212–226.

[27] Karlsson Hibbitt, Inc Sorensen, ABAQUS/Standard user's Manual Volumes I-III and ABAQUS CAE Manual. Version 6.14, Pawtucket (USA) 2014.

[28] J.M. Ricles, R. Sause, P.S. Green, High-strength steel: implications of material and geometric characteristics on inelastic flexural behavior, 20 (4–6) (1998) 323–335.

[29] T. Ma, G. Li, K. Chung, Numerical investigation into high strength Q690 steel columns of welded H-sections under combined compression and bending, J. Constr. Steel Res. 144 (2018) 119–134.

[30] O. Zhao, L. Gardner, B. Young, Behaviour and design of stainless steel SHS and RHS beam-columns, Thin-Walled Struct. 106 (2016) 330–345.

[31] M. Chen, B. Young, Behavior of cold-fromed steel elliptical hollow sections subjected to bending, J. Constr. Steel Res. 158 (2019) 317–330.

[32] M. Su, B. Young, L. Gardner, Continuous beams of aluminum alloy tubular cross-

sections. I: tests and FE model validation, J. Struct. Eng. ASCE 141 (9) (2015) 04014232.

[33] Y. Liang, O. Zhao, Y. Long, L.Gardner, Stainless steel channel sections under combined compression and minor axis bending – part 1: experimental study and numerical modelling, J. Constr. Steel Res. 152 (2019) 154–161.

[34] M. Chen, B. Young, Cross-sectional behavior of cold-fromed steel semi-oval hollow sections, Eng. Struct. 177 (2018) 318–330.

[35] N. Saliba, L. Gardner, Cross-section stability of lean duplex stainless steel welded I-sections, J. Constr. Steel Res. 80 (2013) 1–14.

[36] EN 1993-1-1:2005+A1:2014, Eurocode 3: design of steel structures – part 1.1: General Rules and Rules for Buildings. European Committee for Standardization (CEN), Brussels, 2014.

[37] EN 1993-1-5:2006, Eurocode 3: design of steel structures – part 1.5: Plated Structural Elements. European Committee for Standardization (CEN), Brussels, 2006.

Table 1

Key average material properties measured from longitudinal and transverse coupons [3].

Direction	E (GPa)	f_y (MPa)	f_u (MPa)	ε_u (%)	ε_f (%)	f_u/f_y
Longitudinal	216	702.6	750.3	11	24	1.07
Transverse	202	701.8	765.6	10	24	1.09

Table 2

Membrane residual stress predictive model proposed for S690 welded I-sections [3].

Peak tensile residual stress (f_{wt} or f_{ft})	Peak compressive residual stress (f_{wc} or f_{fc})	a	b	c	d
$0.8f_y$	From equilibrium	$0.225b_f$	$0.15b_f$	$0.075h_w$	$0.225h_w$

Table 3

Measured geometric properties of the tested beam specimens.

Specimen ID	Axis of bending	L (mm)	h (mm)	b_f (mm)	t (mm)	ω_w (mm)	ω_{f1} (mm)	ω_{f2} (mm)	ω_0 (mm)
I-50×50×5-MA	Major axis	495.7	49.44	49.42	4.97	0.04	0.13	0.08	0.13
I-70×70×5-MA		696.5	67.15	69.29	4.93	0.06	0.08	0.08	0.08
I-80×60×5-MA		693.7	79.39	59.01	4.96	0.03	0.14	0.11	0.14
I-90×70×5-MA		698.1	90.35	69.20	4.93	0.06	0.11	0.10	0.11
I-100×100×5-MA		998.5	99.02	99.09	4.91	0.05	0.15	0.13	0.15
I-140×70×5-MA		1397.3	139.33	69.23	4.94	0.04	0.09	0.08	0.09
I-50×50×5-MI	Minor axis	497.5	49.41	49.59	4.99	0.04	0.09	0.10	0.10
I-70×70×5-MI		874.0	68.62	69.28	4.97	0.07	0.12	0.07	0.12
I-80×60×5-MI		696.0	79.63	59.16	4.90	0.06	0.13	0.13	0.13
I-90×70×5-MI		756.0	90.35	69.12	4.93	0.06	0.09	0.13	0.13
I-100×100×5-MI		996.5	99.31	99.48	4.98	0.05	0.15	0.13	0.15
I-140×70×5-MI		1397.5	139.59	68.98	4.94	0.09	0.07	0.10	0.10

Table 4

Test results for beam specimens.

Specimen ID	Bending axis	M_u (kNm)	M_u/M_{pl}	M_u/M_{el}	R
I-50×50×5-MA	Major axis	10.0	1.10	1.30	>1.61
I-70×70×5-MA		19.4	1.09	1.25	>4.04
I-80×60×5-MA		21.0	1.07	1.24	>2.41
I-90×70×5-MA		27.7	1.07	1.22	2.68
I-100×100×5-MA		39.8	1.02	1.15	1.48
I-140×70×5-MA		49.5	1.06	1.24	2.78
I-50×50×5-MI	Minor axis	5.0	1.11	1.73	>4.15
I-70×70×5-MI		9.3	1.08	1.66	>6.13
I-80×60×5-MI		6.8	1.08	1.69	>6.16
I-90×70×5-MI		9.2	1.07	1.67	>5.35
I-100×100×5-MI		17.2	0.98	1.49	–*
I-140×70×5-MI		10.0	1.10	1.80	>8.76

* The ultimate moment M_u of the specimen I-100×100×5-MI is lower than the cross-section plastic moment capacity M_{pl}.

Table 5

Comparison of experimental results with FE results considering four levels of imperfections.

Specimen ID	Finite element M_u / Test M_u			
	ω_0	$t/100$	$t/30$	$t/10$
I-50×50×5-MA	0.98	0.98	0.98	0.97
I-70×70×5-MA	0.95	0.95	0.94	0.94
I-80×60×5-MA	0.97	0.98	0.97	0.95
I-90×70×5-MA	1.01	1.02	1.01	1.00
I-100×100×5-MA	0.97	0.98	0.97	0.95
I-140×70×5-MA	1.00	1.00	0.99	0.98
I-50×50×5-MI	1.02	1.03	1.01	0.97
I-70×70×5-MI	0.96	0.98	0.95	0.89
I-80×60×5-MI	0.93	0.94	0.93	0.90
I-90×70×5-MI	0.91	0.91	0.89	0.86
I-100×100×5-MI	0.96	0.98	0.95	0.92
I-140×70×5-MI	0.96	0.97	0.94	0.90
Mean	0.97	0.98	0.96	0.94
COV	0.03	0.03	0.03	0.05

Table 6
Comparisons of experimental and FE ultimate moments against predicted bending moment resistances.

(a) EN 1993-1-12 [14]

Axis of bending	Class of cross-section	Number of experimental data	Number of numerical data	$M_u/M_{u,EC3}$	
				Mean	COV
Major axis	Class 1 or Class 2 I-section	5	34	1.07	0.02
	Class 3 I-section	0	59	1.15	0.04
	Class 4 I-section	1	92	1.28	0.08
	Sub-total	6	185	1.18	0.09
Minor axis	Class 1 and 2 I-section	5	25	1.09	0.02
	Class 3 I-section	1	26	1.57	0.05
	Class 4 I-section	0	56	1.52	0.06
	Sub-total	6	101	1.44	0.19
	Total	12	286	1.26	0.18

(b) AS 4100 [15]

Axis of bending	Class of cross-section	Number of experimental data	Number of numerical data	$M_u/M_{u,AS}$	
				Mean	COV
Major axis	Compact I-section	2	21	1.08	0.01
	Non-compact I-section	4	80	1.10	0.03
	Slender I-section	0	84	1.58	0.29
	Sub-total	6	185	1.31	0.31
Minor axis	Compact I-section	2	8	1.17	0.03
	Non-compact I-section	4	51	1.33	0.06
	Slender I-section	0	42	3.22	1.46
	Sub-total	6	101	2.05	1.38
	Total	12	286	1.57	0.92

(c) ANSI/AISC 360-16 [16]

Axis of bending	Class of cross-section	Number of experimental data	Number of numerical data	$M_u/M_{u,AISC}$	
				Mean	COV
Major axis	Compact I-section	2	36	1.06	0.02
	Non-compact I-section	4	131	1.11	0.07
	Slender I-section	0	18	1.35	0.15
	Sub-total	6	185	1.12	0.10
Minor axis	Compact I-section	2	28	1.09	0.03
	Non-compact I-section	4	40	1.30	0.16
	Slender I-section	0	33	3.13	1.08
	Sub-total	6	101	1.81	1.11
	Total	12	286	1.36	0.74

Table 7

Established slenderness limits in the current design standards.

(a) EN 1993-1-12 [14]

Plate element type	Loading condition	Class 3 limit	Class 2 limit
Outstand flange	Compression	$14\varepsilon_{EC3}$	$10\varepsilon_{EC3}$
Internal web	Bending	$124\varepsilon_{EC3}$	$83\varepsilon_{EC3}$
Outstand flange	Compressive stress gradient	$21\varepsilon_{EC3}k_{\sigma}^{0.5}$	–

(b) AS 4100 [15]

Plate element type	Loading condition	Yield slenderness limit	Plasticity slenderness limit
Outstand flange	Compression	$14\varepsilon_{AS}$	$8\varepsilon_{AS}$
Internal web	Bending	$115\varepsilon_{AS}$	$82\varepsilon_{AS}$
Outstand flange	Compressive stress gradient	$22\varepsilon_{AS}$	–

(c) ANSI/AISC 360-16 [16]

Plate element type	Loading condition	Non-compact limiting width-to-thickness ratio	Compact limiting width-to-thickness ratio
Outstand flange	Compression	$1.14\varepsilon_{AISC}k_c^{0.5}$	$0.38\varepsilon_{AISC}$
Internal web	Bending	$5.7\varepsilon_{AISC}$	$3.76\varepsilon_{AISC}$
Outstand flange	Compressive stress gradient	$1.0\varepsilon_{AISC}$	–

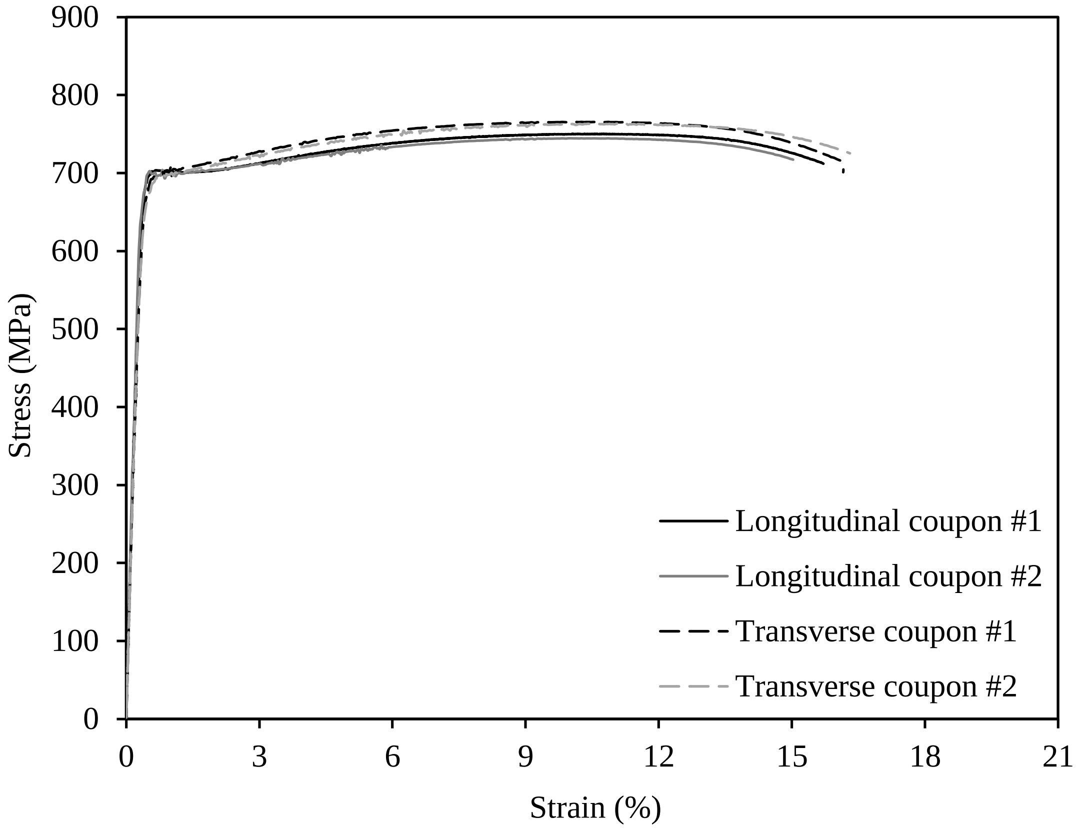

Fig. 1. Measured **s**tress–strain curves from longitudinal and transverse coupons [3].

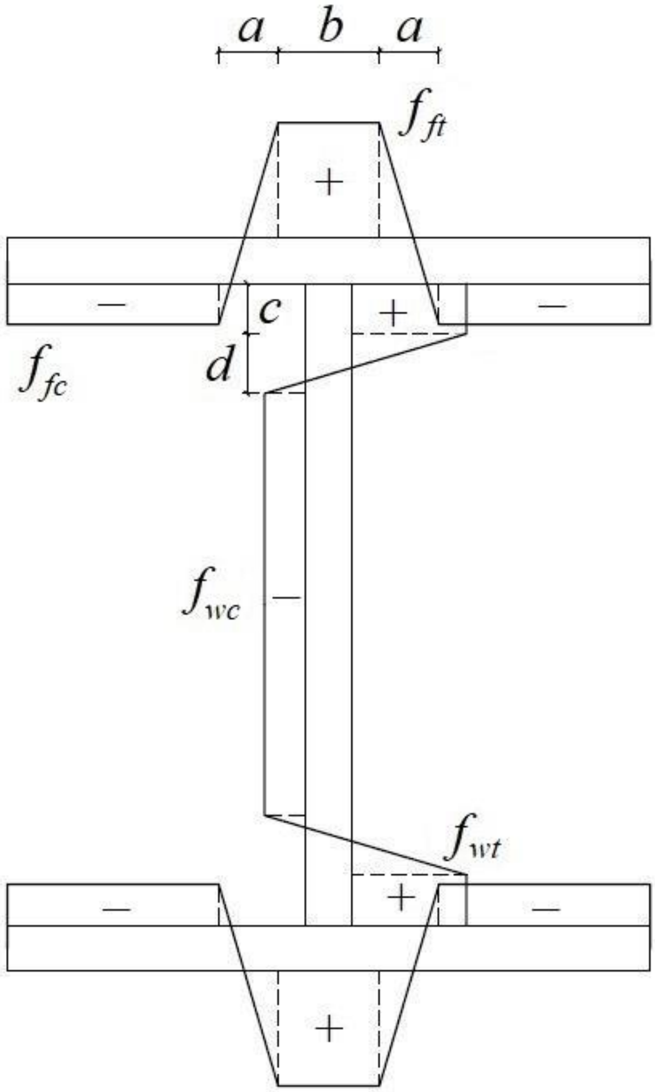

Fig. 2. General membrane residual stress pattern for welded I-sections [3].

Fig. 3. Test rig for initial local geometric imperfection measurements.

Fig. 4. Minor-axis four-point bending test setup.

Fig. 5. Major-axis four-point bending test setup.

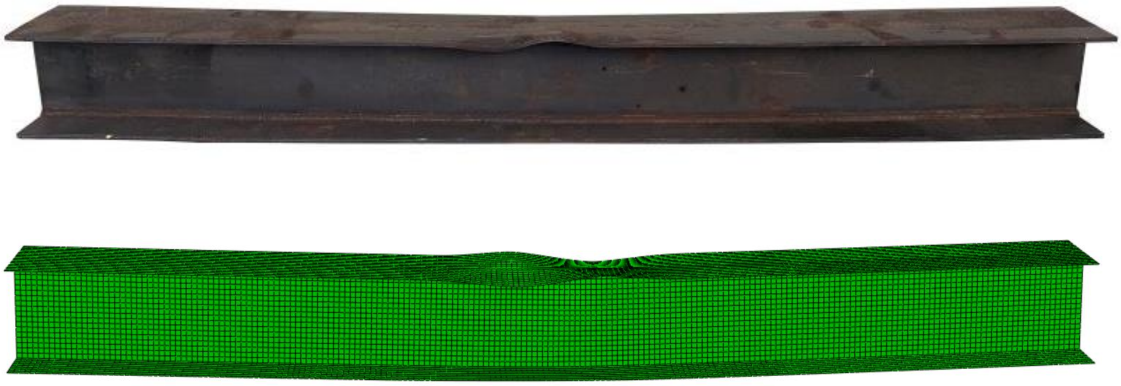

Fig. 6. Test and FE failure modes for beam specimen I-100×100×5-MA in major-axis bending.

Fig. 7. Test and FE failure modes for beam specimen I-100×100×5-MI in minor-axis bending.

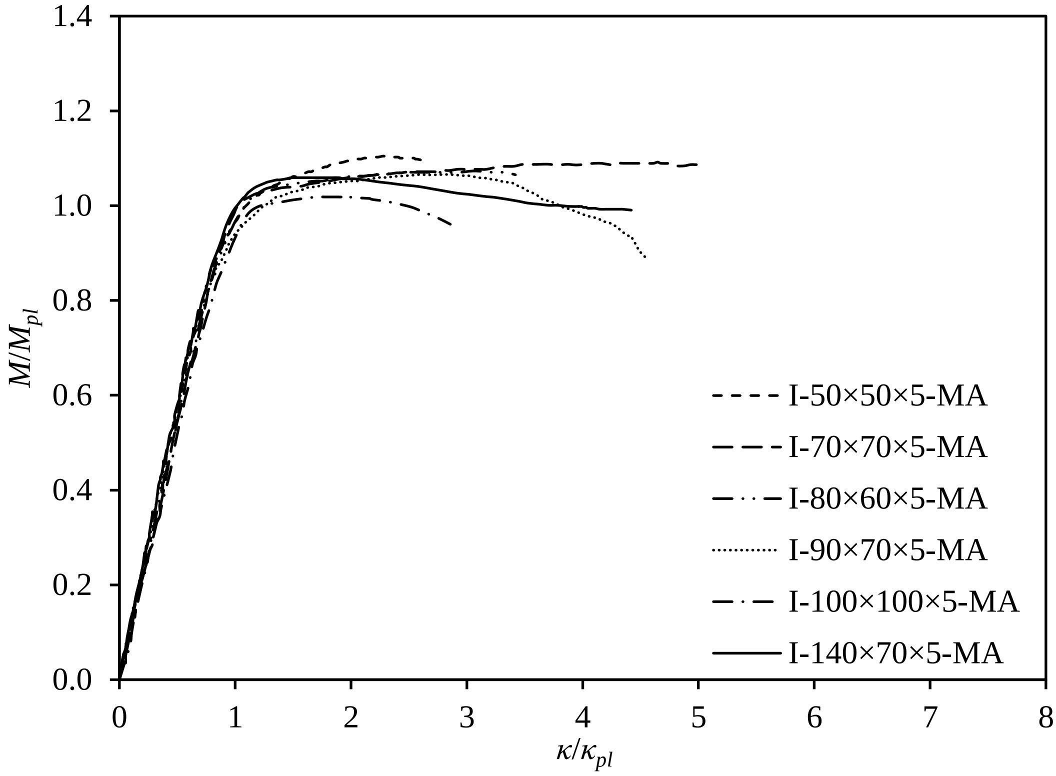

Fig. 8. Normalised moment–curvature curves for beam specimens bent about the major principal axes.

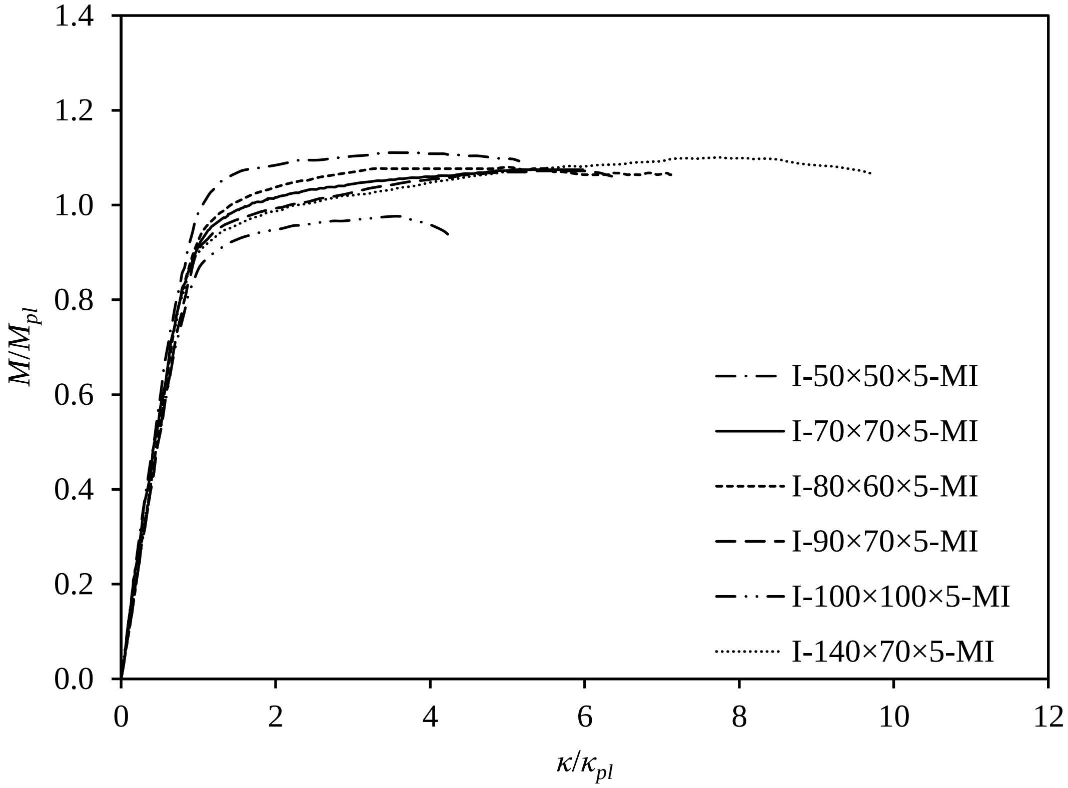

Fig. 9. Normalised moment–curvature curves for beam specimens bent about the minor principal axes.

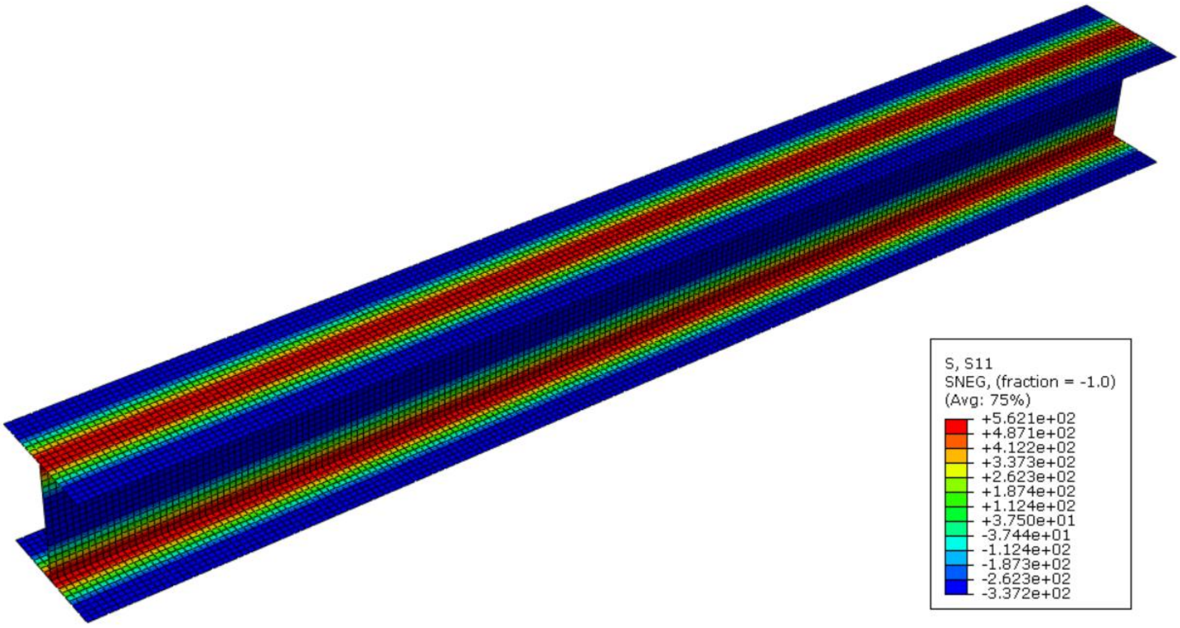

Fig. 10. Typical residual stress pattern (in MPa) in modelled S690 welded I-section beams I-100×100×5-MA and I-100×100×5-MI (Positive values indicate tensile residual stresses while negative values indicate compressive residual stresses).

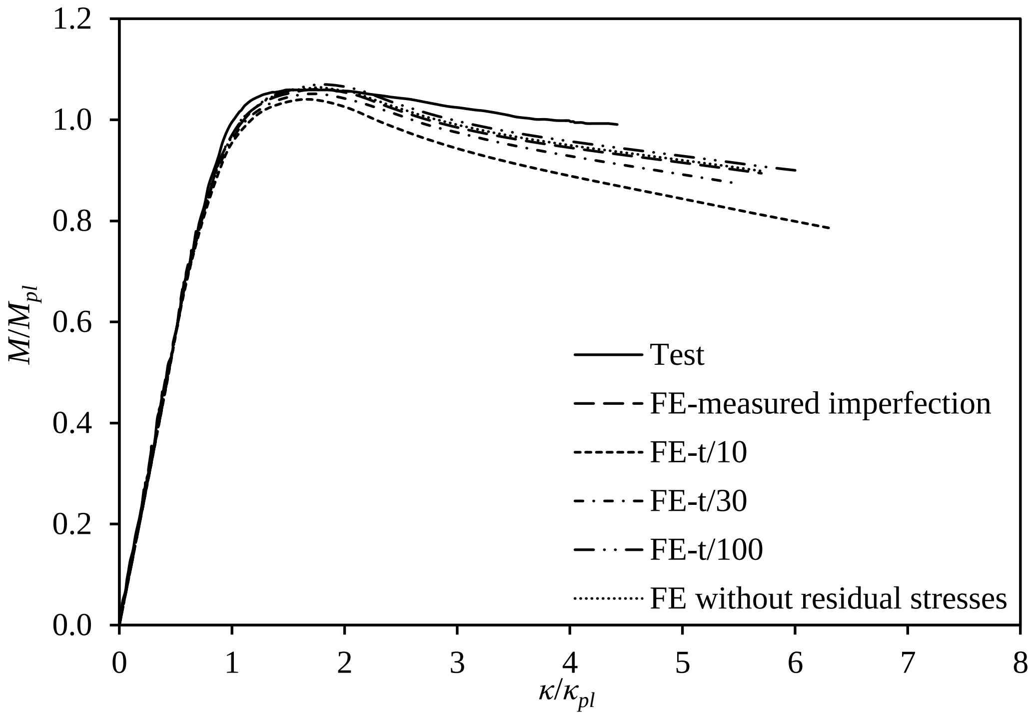

Fig. 11. Normalised test and FE moment–curvature curves for beam specimen I-140×70×5-MA.

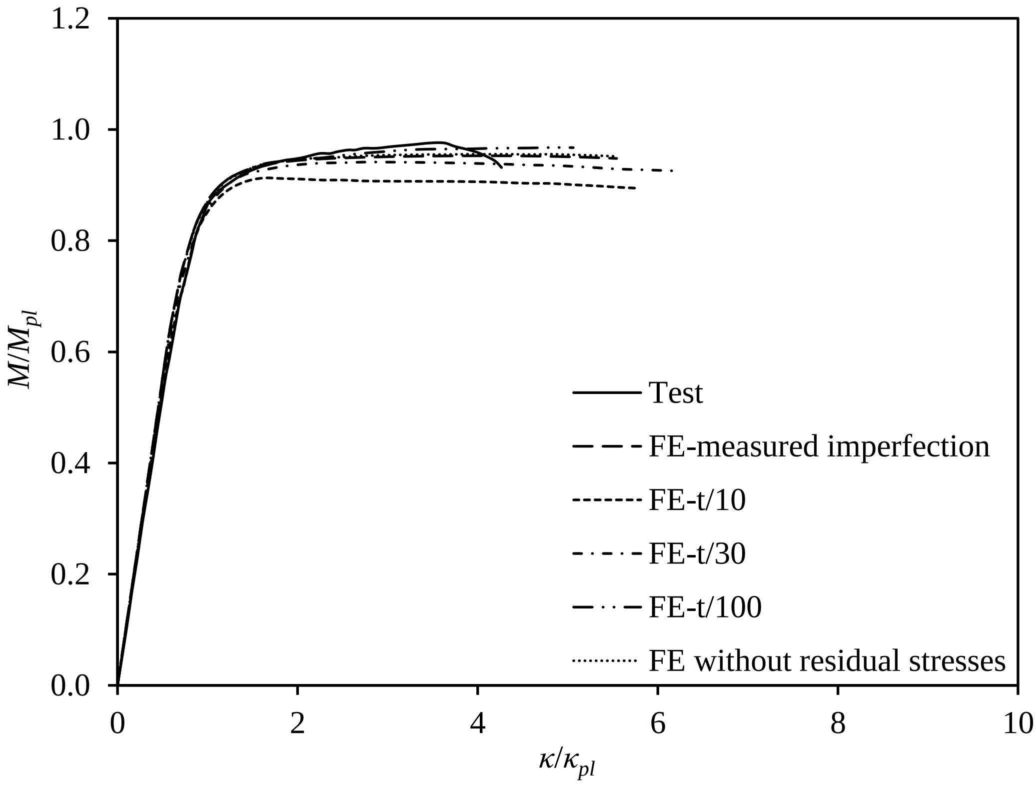

Fig. 12. Normalised test and FE moment–curvature curves for beam specimen I-100×100×5-MI.

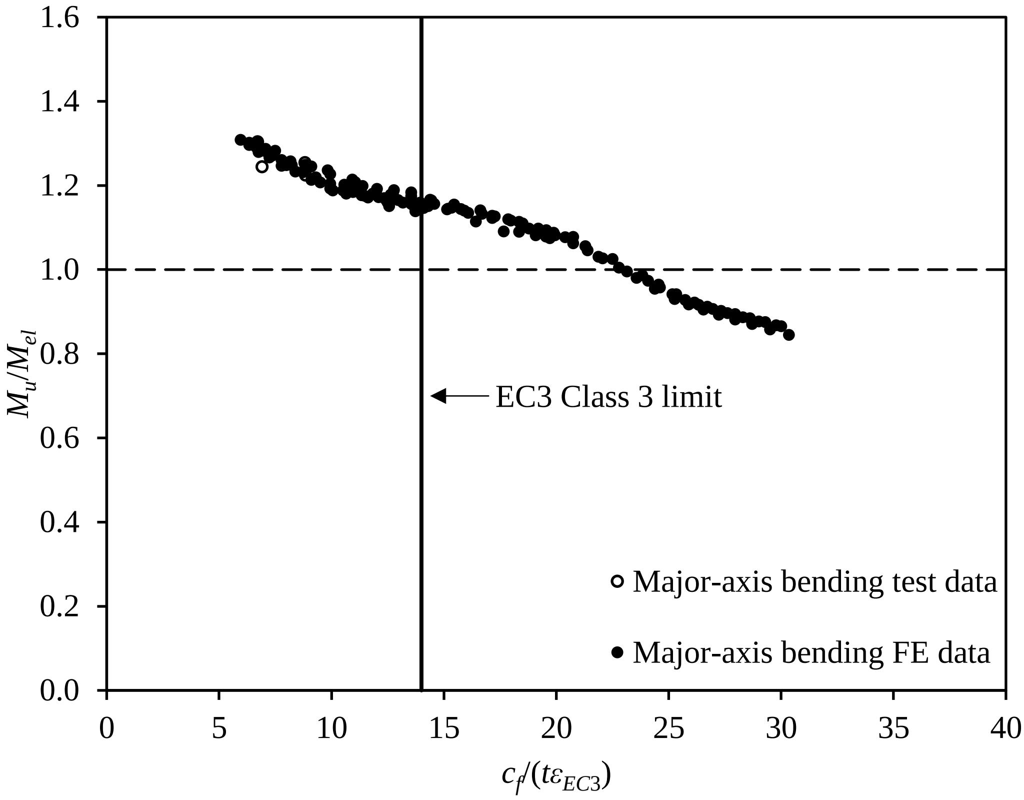

Fig. 13. EC3 Class 3 slenderness limit for outstand elements in compression.

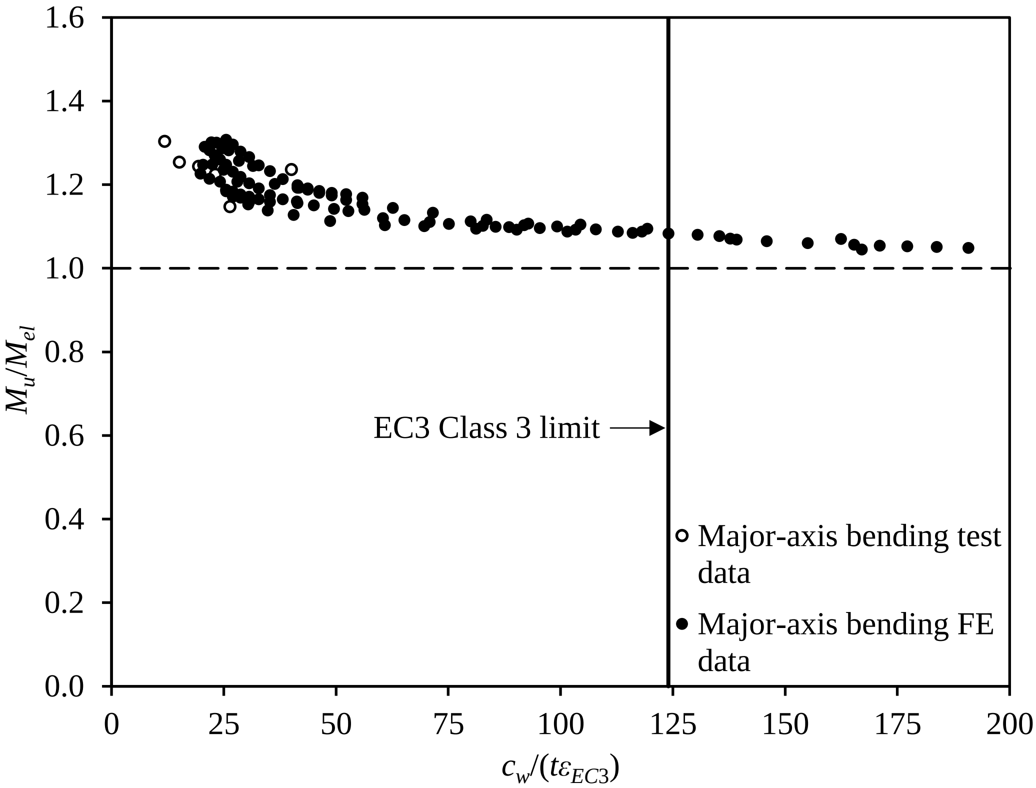

Fig. 14. EC3 Class 3 slenderness limit for internal elements in bending.

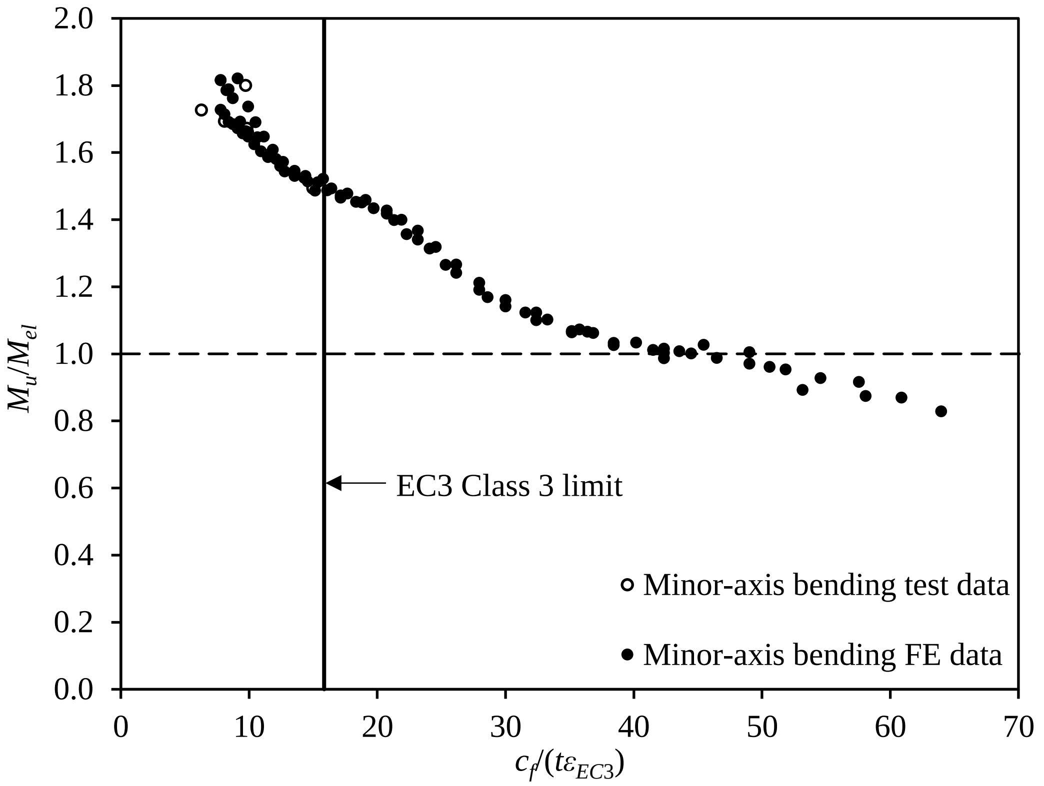

Fig. 15. EC3 Class 3 slenderness limit for outstand elements under triangular compressive stress gradients.

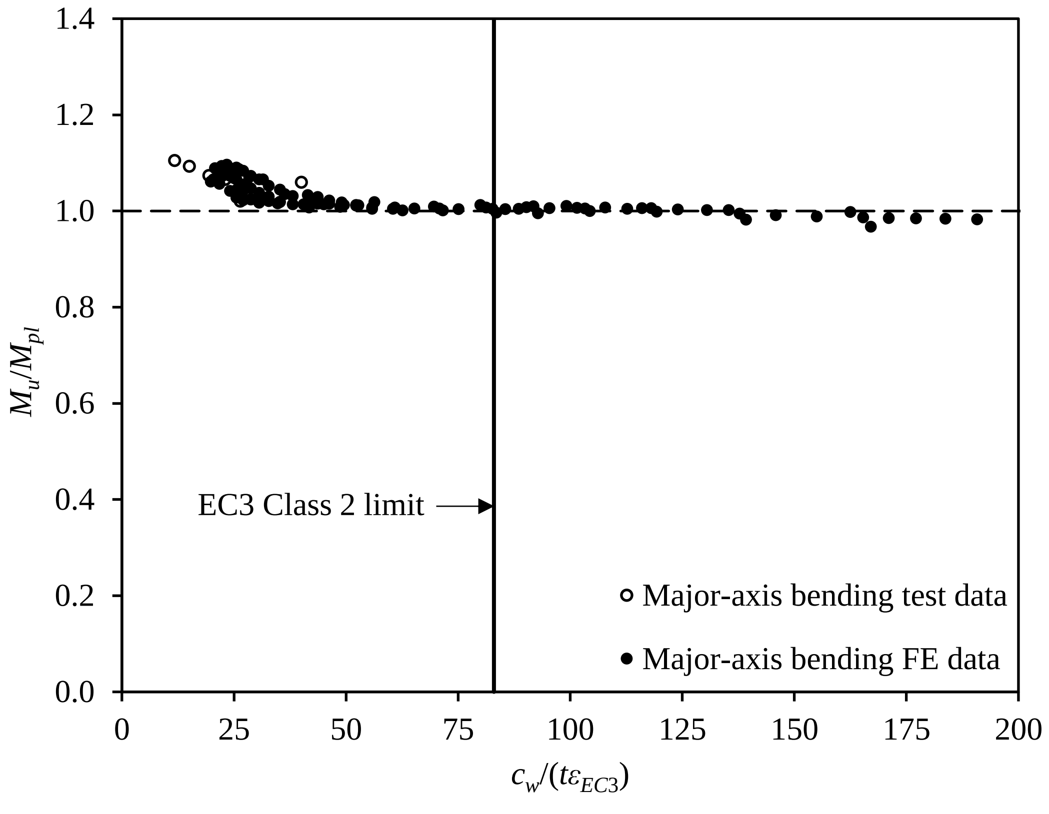

Fig. 16. EC3 Class 2 slenderness limit for internal elements in bending.

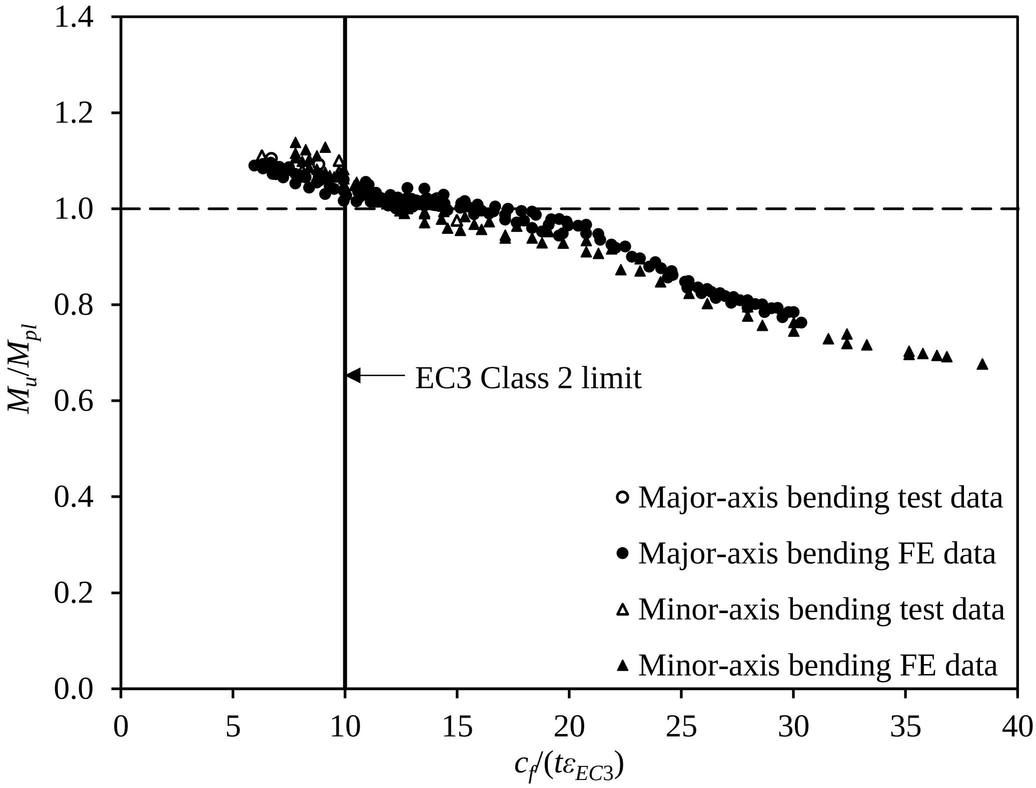

Fig. 17. EC3 Class 2 slenderness limit for outstand elements in compression.

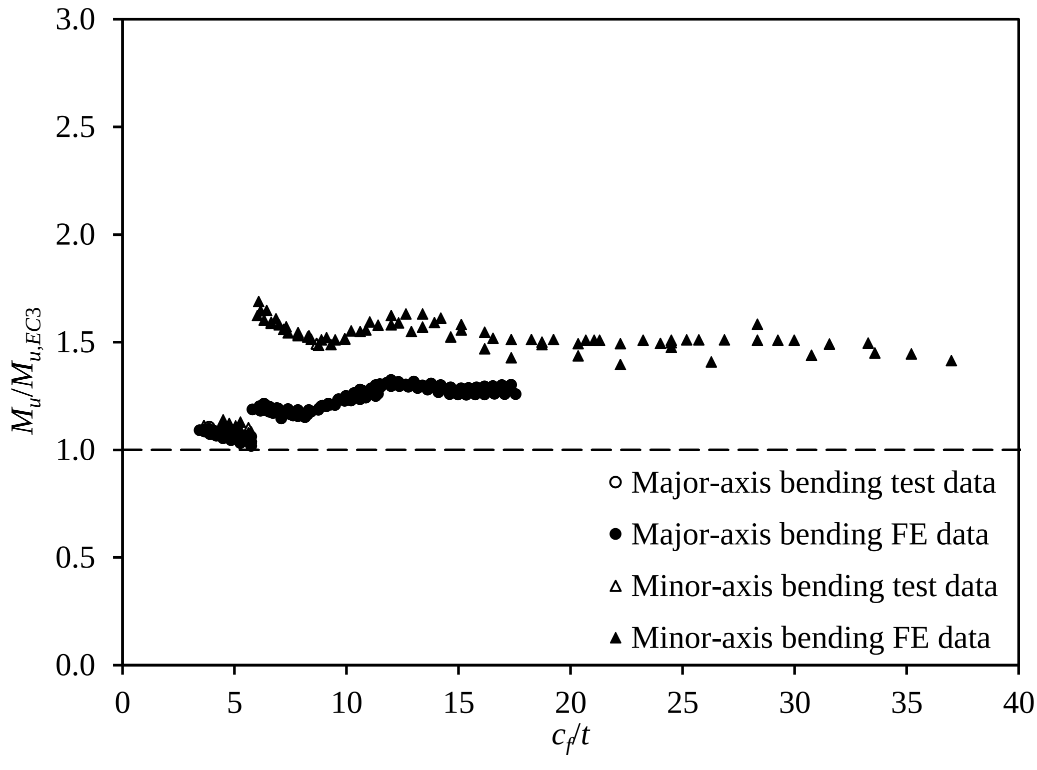

Fig. 18. Comparison of experimental and numerical ultimate moments with EC3 bending resistance predictions.

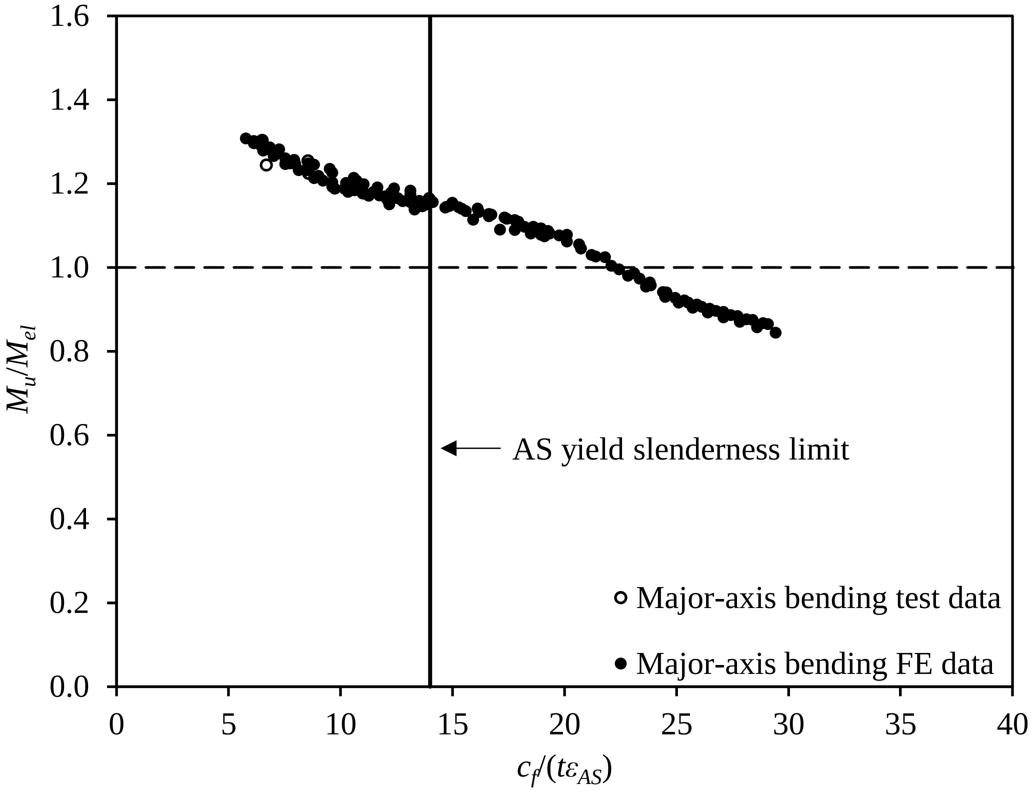

Fig. 19. AS yield slenderness limit for outstand elements in compression.

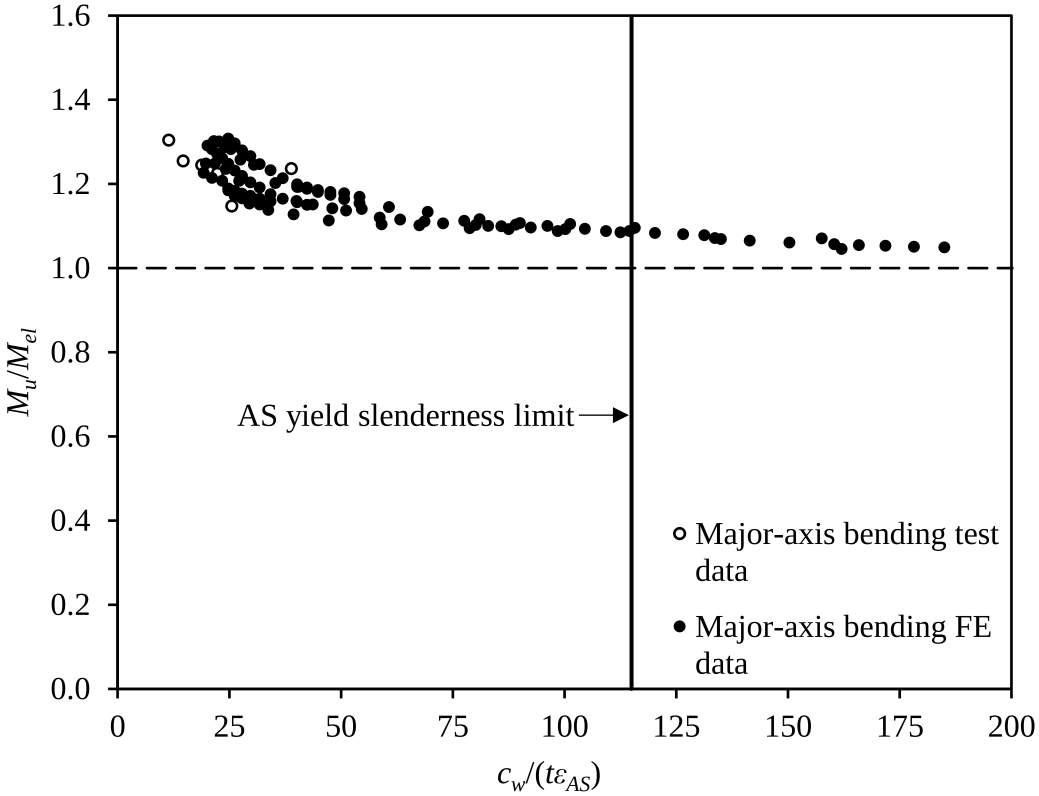

Fig. 20. AS yield slenderness limit for internal elements in bending.

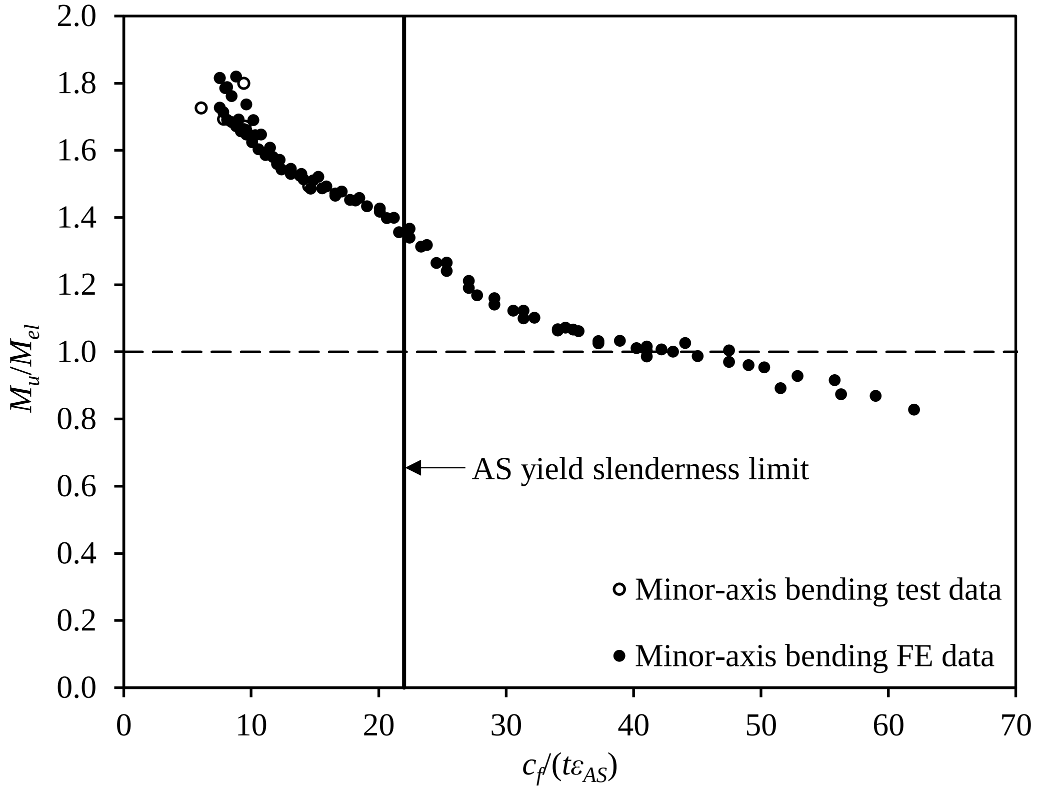

Fig. 21. AS yield slenderness limit for outstand elements under triangular compressive stress gradients.

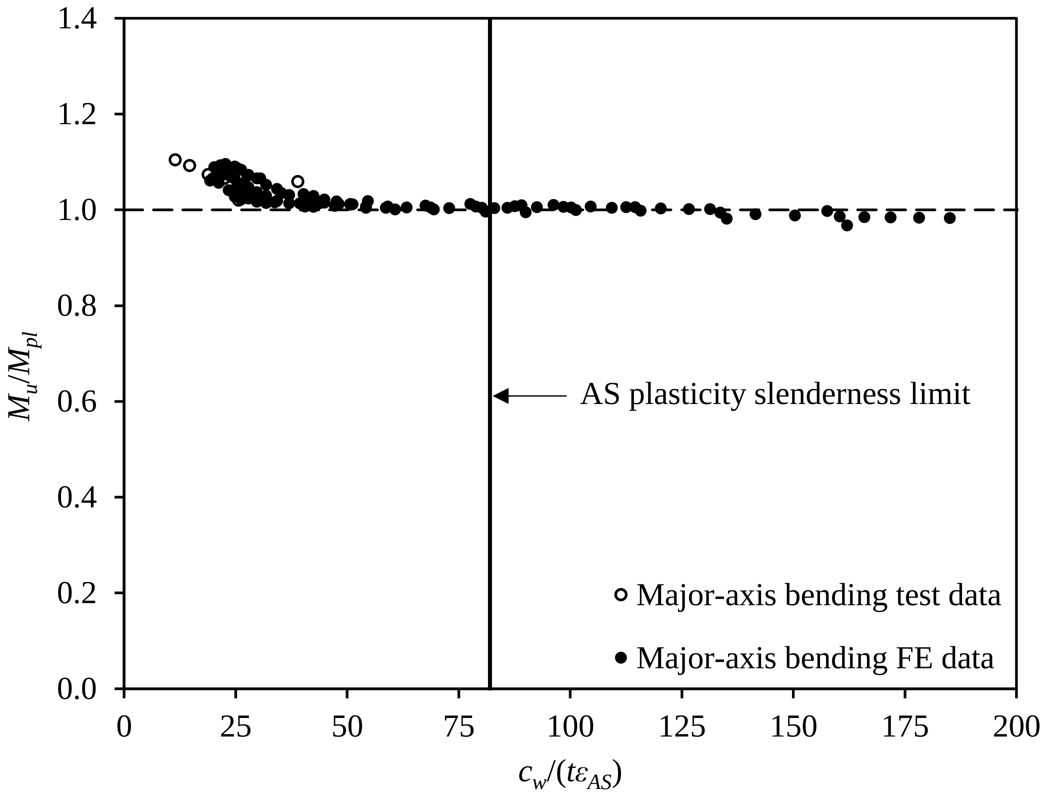

Fig. 22. AS plasticity slenderness limit for internal elements in bending.

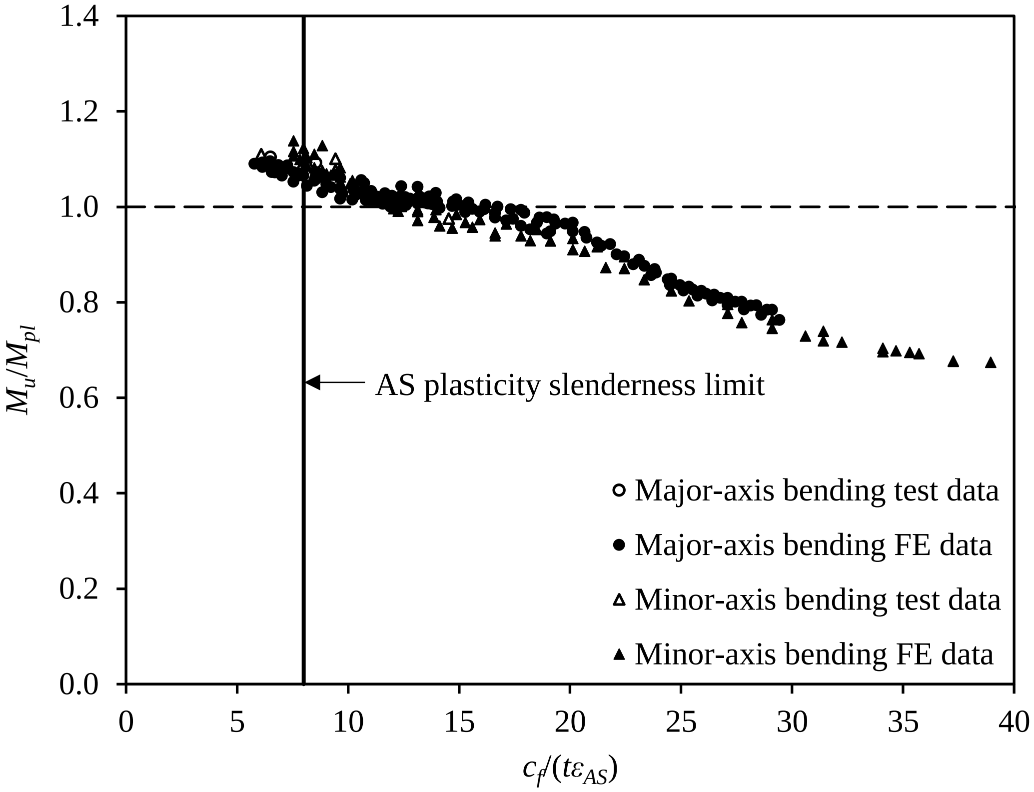

Fig. 23. AS plasticity slenderness limit for outstand elements in compression.

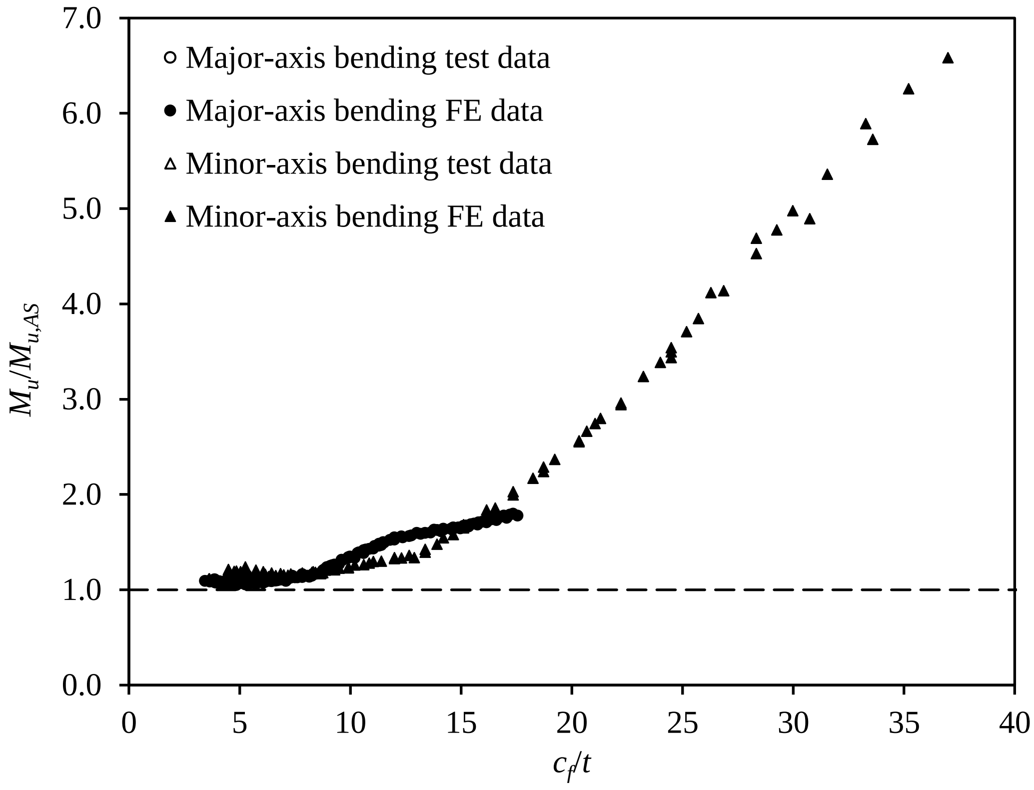

Fig. 24. Comparison of experimental and numerical ultimate moments with AS bending resistance predictions.

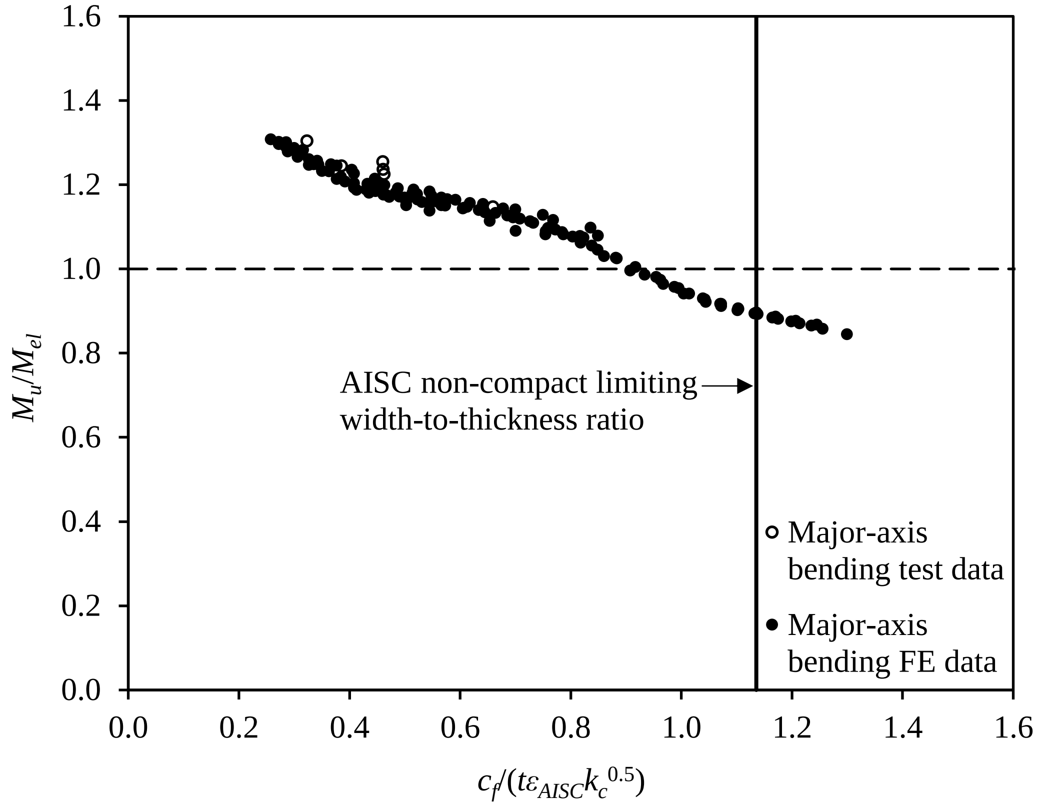

Fig. 25. AISC non-compact limiting width-to-thickness ratio for outstand elements in compression.

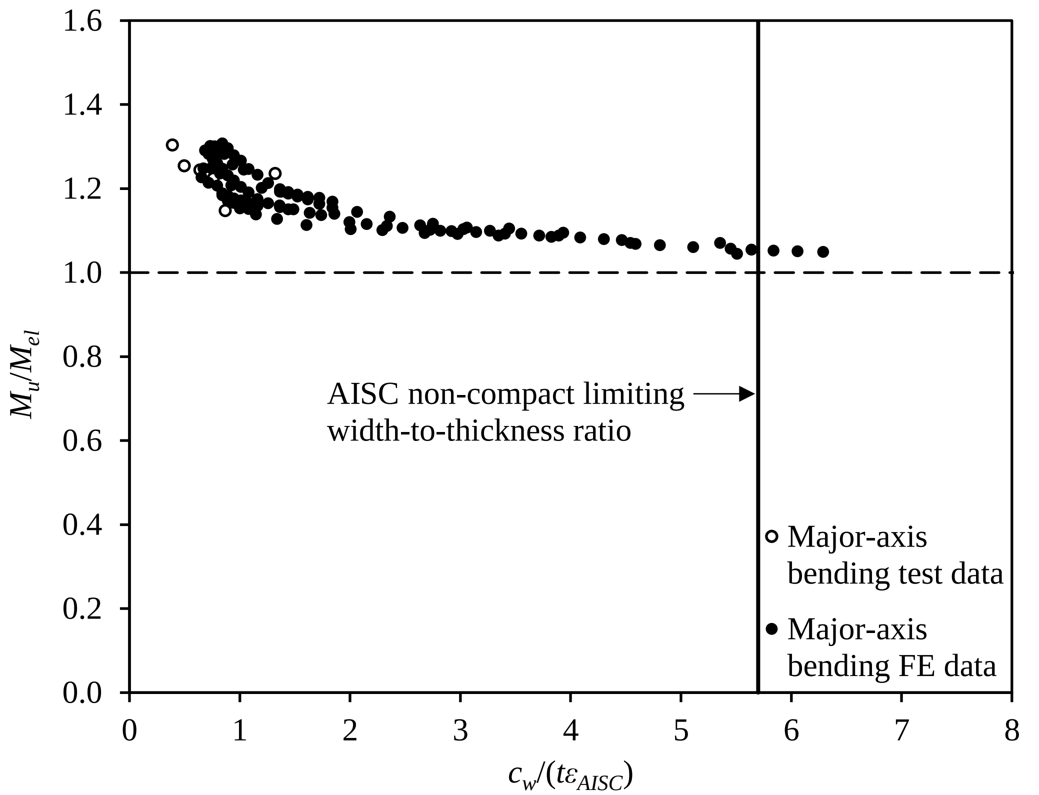

Fig. 26. AISC non-compact limiting width-to-thickness ratio for internal elements in bending.

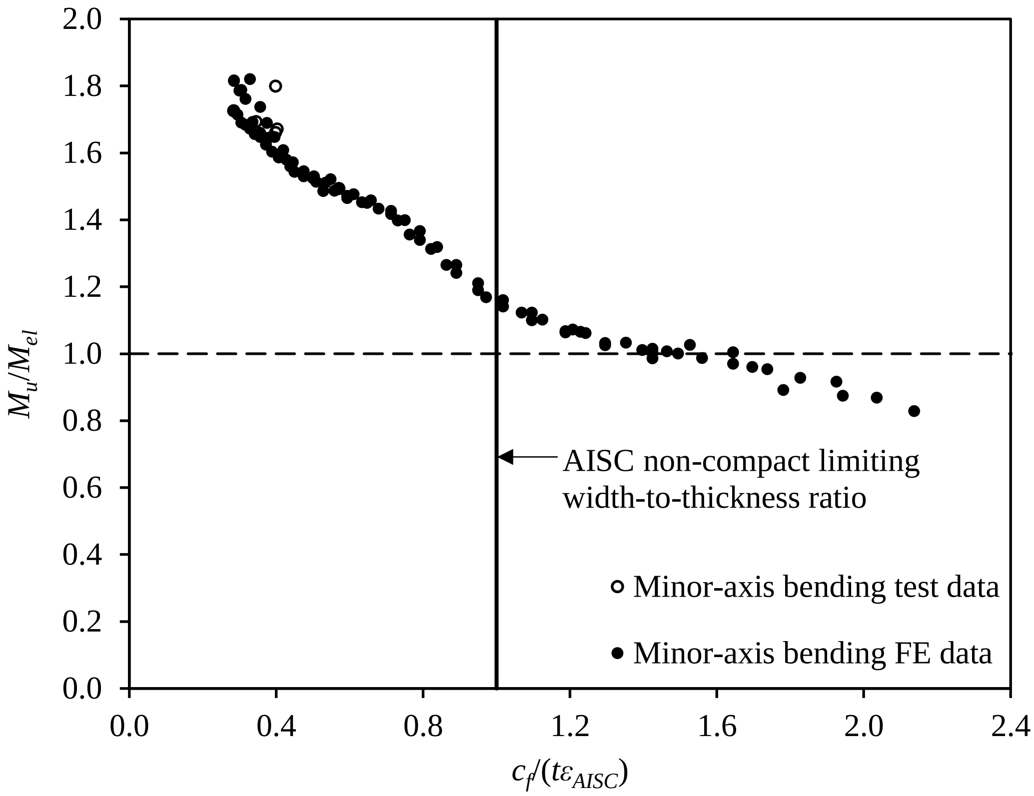

Fig. 27. AISC non-compact limiting width-to-thickness ratio for outstand elements under triangular compressive stress gradients.

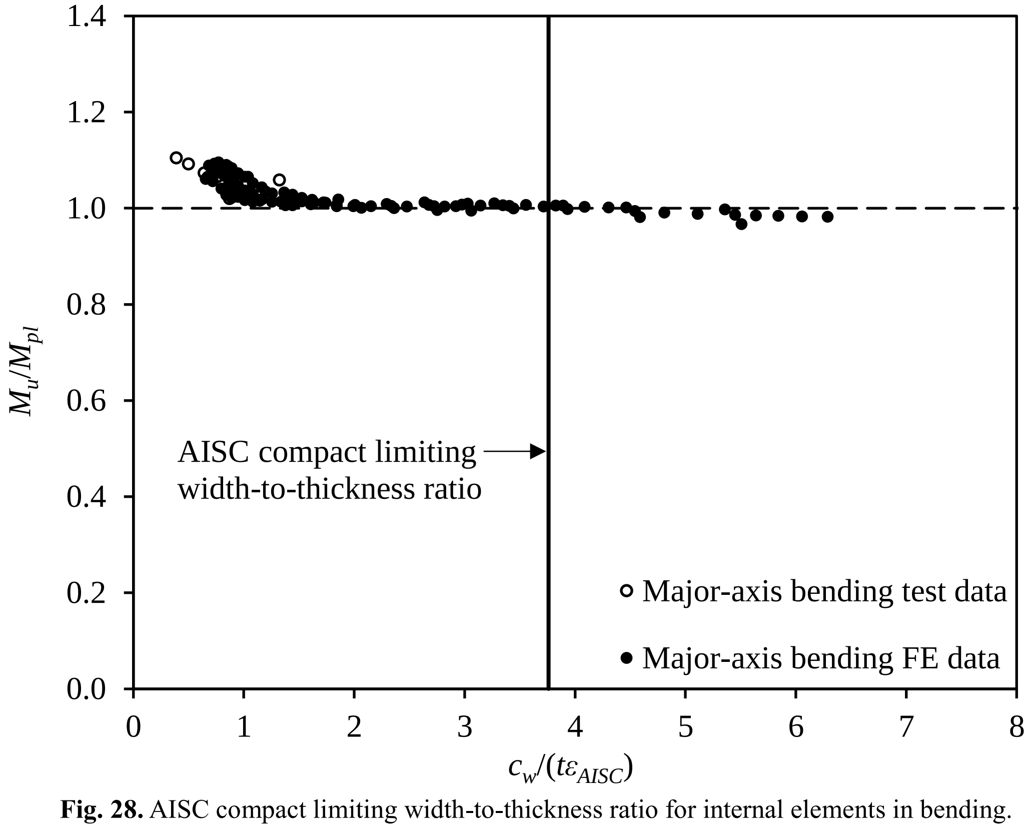

Fig. 28. AISC compact limiting width-to-thickness ratio for internal elements in bending.

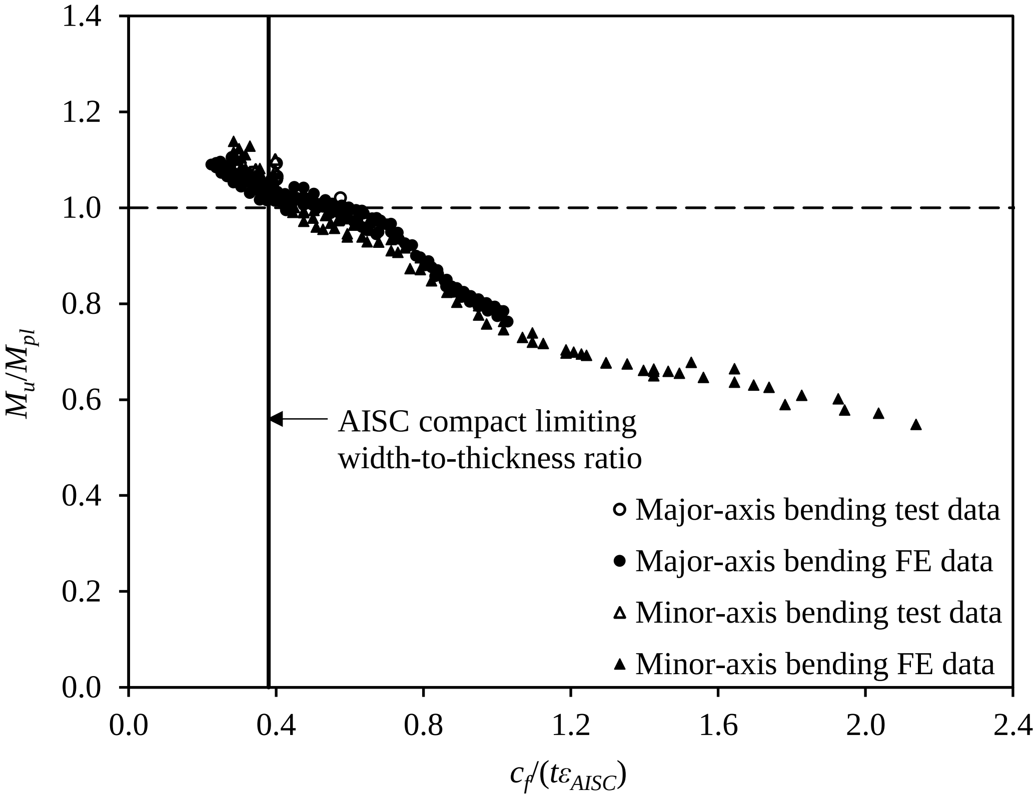

Fig. 29. AISC compact limiting width-to-thickness ratio for outstand elements in compression.

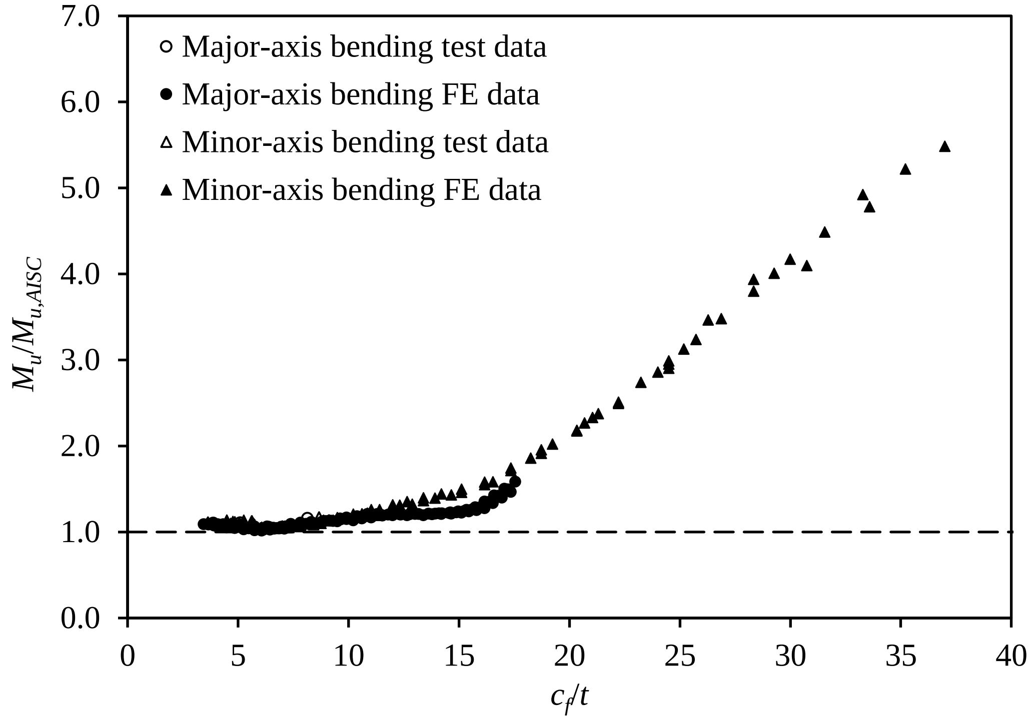

Fig. 30. Comparison of experimental and numerical ultimate moments with AISC bending resistance predictions.